Articles in PresS. J Neurophysiol (August 15, 2012). doi:10.1152/jn.00914.2011



# Network and neuronal membrane properties in hybrid networks reciprocally regulate selectivity to rapid thalamocortical inputs

Michael J. Pesavento[1], David J Pinto[1,2,3]

[1]Department of Neurobiology and Anatomy
[2]Department of Biomedical Engineering
[3]Department of Neurology
University of Rochester School of Medicine
Rochester, NY 14642

Running Title: Network and membrane properties in hybrid network

Corresponding Author:

Michael J. Pesavento
Department of Physics, 0374
University of California, San Diego
9500 Gilman Dr.
La Jolla, CA 92093-0374
Email: mpesavento@ucsd.edu

Number of figures: 11 (10 color) + 1 table
Number of words,
Abstract: 250
Introduction: 1303
Discussion: 3094

Keywords: thalamocortical transformation; barrel cortex; somatosensory cortex; neural circuit; feedforward inhibition; recurrent excitation

Acknowledgements: We would like to thank J. S. Connell for technical assistance with software architecture. Thank you for helpful comments given by David Kleinfeld and Daniel Simons. This work was supported by an NSF Career Award (DJP).

## ABSTRACT

Rapidly changing environments require rapid processing from sensory inputs. Varying deflection velocities of a rodent's primary facial vibrissa cause varying temporal neuronal activity profiles within the ventral posteromedial thalamic nucleus. Local neuron populations in a single somatosensory layer 4 barrel transform sparsely coded input into a spike count based on the input's temporal profile. We investigate this transformation by creating a barrel-like hybrid network with whole-cell recordings of *in vitro* neurons from a cortical slice preparation, embedding the biological neuron in the simulated network by presenting virtual synaptic conductances via a conductance clamp. Utilizing the hybrid network, we examine the reciprocal network properties (local excitatory and inhibitory synaptic convergence), and neuronal membrane properties (input resistance) by altering the barrel population response to diverse thalamic input. In the presence of local network input, neurons are more selective to thalamic input timing; this arises from strong feedforward inhibition. Strongly inhibitory (damping) network regimes are more selective to timing and less selective to the magnitude of input, but require stronger initial input. Input selectivity relies heavily on the different membrane properties of excitatory and inhibitory neurons. When inhibitory and excitatory neurons have identical membrane properties, the sensitivity of *in vitro* neurons to temporal versus magnitude features of input was substantially reduced. Increasing the mean leak conductance of the inhibitory cells decreased the network's temporal sensitivity, whereas increasing excitatory leak conductance enhanced magnitude sensitivity. Local network synapses are essential in shaping thalamic input, and differing membrane properties of functional classes reciprocally modulate this effect.

## INTRODUCTION

Understanding the relationship between single neuron membrane properties and network processing is a necessary component of understanding neuronal circuit processing. Many studies have examined the response of cortical neurons to sensory stimuli within networks (*in vivo* whole-animal preparations), while others have examined the activity of such neurons responding to injected current in relative isolation (*in vitro* slice preparations). Due to the difficulty in separating the roles of network connectivity and neuronal membrane properties in reshaping transient input, this relationship requires an innovative approach. We create a hybrid network – consisting of a biological neuron embedded in a simulated conductance-based computational network – to assist in the isolation of neuronal and network contributions to reshaping transient input. This technique gives unprecedented levels of control over network connectivity and neuronal membrane properties while permitting comparison of *in vitro* neuron responses across a multitude of conditions.

The rodent vibrissa system is uniquely positioned to provide insight into neuronal- and network-level processing of sensory inputs. Discrete, dense, clusters of neurons within layer 4 of rodent primary somatosensory cortex, known as "barrels" (Woolsey and Van der Loos, 1970; Welker, 1971), receive the majority of their afferent input from analogous groups of neurons in the ventral posteromedial (VPM) nucleus in the thalamus (Jensen and Killackey, 1987; Simons and Carvell, 1989; Land et al., 1995). Within a layer 4 barrel, three electrophysiologically distinct neuronal subpopulations form a strongly interconnected synaptic network: excitatory regular-spiking (RS) neurons, inhibitory fast-spiking (FS) neurons, and inhibitory low-threshold-spiking (LTS) neurons (McCormick et al., 1985; Beierlein et al., 2003). Although several neuronal morphologies have been observed in each class (Kawaguchi, 1993; Kawaguchi and Kubota, 1997; Staiger et al., 2004; Sun et al., 2006), electrophysiological measures allow accurate classification by observed intrinsic membrane properties in response to square pulses of current injection (Pesavento et al., 2010; Gibson et al., 1999; McCormick et al., 1985). In this study, we are

78 focusing on RS and FS neuron transient responses to thalamic input; LTS neurons largely do not receive
79 direct thalamic input (Cruikshank et al., 2010; Gibson et al., 1999) and therefore are not discussed here.

80 The temporal features of sensory stimuli are conveyed through the thalamus to the sensory cortex
81 via multiple sensory modalities (Phillips et al., 1988; Buracas et al., 1998; DeWeese et al., 2003; Reinagel
82 and Reid, 2000; Wehr and Zador, 2003). A number of studies have examined the contribution of either
83 cortical neurons or cortical networks in shaping the responses to rapid thalamic input. Layer 4 barrel
84 neurons respond preferentially to fast, synchronous or near-synchronous thalamic input (Pinto et al.,
85 2000; Ito and Kato, 2002; Wilent and Contreras, 2004; Arabzadeh et al., 2005), while similar results have
86 been reported in both visual cortex (Alonso et al., 1996; Hirsch et al., 2008) and auditory cortex (Wehr
87 and Zador, 2003). This sensitivity may be due in part to the membrane properties of individual neurons
88 (Chung and Ferster, 1998; Azouz and Gray, 2000; Wilent and Contreras, 2005; Pesavento et al., 2010).
89 Several studies also suggest that network interactions contribute to barrel response sensitivity (Pinto et al.,
90 2000; Wilent and Contreras, 2004; Arabzadeh et al., 2005). Our goal is to clarify these reciprocal
91 contributions of neuronal and network properties in context of temporal selectivity in the barrel system.

92 Neurons within the barrel form an interconnected synaptic network, including direct thalamic
93 input (Jensen and Killackey, 1987), feedforward inhibition (Miller et al., 2001; Pouille and Scanziani,
94 2001; Swadlow and Gusev, 2002; Wehr and Zador, 2003; Lawrence and McBain, 2003; Gabernet et al.,
95 2005; Bruno and Sakmann, 2006; Cruikshank et al., 2007), and recurrent excitation (Douglas et al., 1995;
96 Adorjan et al., 1999; Miller et al., 2001). In barrels, the overall effect of network interactions is inhibitory
97 or damping due to the strength of feedforward inhibition (Pinto et al., 2003; Swadlow et al., 2005). We
98 further explore how each class of synaptic inputs – thalamic, local excitatory, and local inhibitory –
99 contribute to modifying neuronal response properties. Previous modeling studies have explored the
100 balance of local and thalamic inputs (Kyriazi and Simons, 1993) and excitation and inhibition within the
101 local network (Pinto et al., 2003). The role of network feedback has also been examined via bath
102 application of muscimol, effectively inhibiting all local synaptic connections (Liu et al., 2007). However,

this likely alters the intrinsic membrane properties of the neurons, making an accurate comparison difficult. The hybrid network is well suited to the task of comparing the responses of a single neuron or neuronal population in the absence of local network input versus the presence of network input. An additional strength of the hybrid network over modeling studies is that we are examining the responses of biological neurons.

Previously, we characterized the activity of individual neurons in rat barrel cortex in response to simulated thalamocortical input (Pesavento et al., 2010). We found that neurons responding in the absence of local network activity cannot account for the response sensitivity of ensemble barrel responses observed *in vivo* (Pinto et al., 2000). In this study, we examine the combined effect of intrinsic neuronal and network properties using a unique combination of whole-cell patch recordings and real-time computer simulations. Recording from individual barrel neurons *in vitro*, we use a conductance clamp to embed the neurons in a simulated barrel network. This arrangement allows us to change the intrinsic properties of the barrel neurons and examine the effects of those changes on the network's response. Our hybrid network is activated by simulated thalamic synaptic inputs modeled after real thalamic responses to whisker deflections of different velocities (Pesavento et al., 2010; Pinto et al., 2000).

Using the hybrid network, we find that the presence of local synaptic input from the surrounding network explains much of the difference of response measures between *in vivo* neurons and *in vitro* neurons. We then examine what aspects of the network contribute to shaping response selectivity to thalamic input, and how these principles can apply to other sensory modalities. Damping networks (Pinto et al., 2003) with strong feedforward inhibition enhance response selectivity to fast inputs while decreasing the sensitivity to input magnitude. Recurrent excitation may play an important role in non-transient input processing.

The intrinsic membrane properties of neurons – such as input resistance and firing rate adaptation – have been used to classify electrophysiological differences between subpopulations; however, it is also

important to note that these classifications also distinguish between different functional classifications, such as excitatory and inhibitory synaptic projections. Excitatory RS neurons have higher input resistance than inhibitory FS neurons, which results in broader response selectivity in the inhibitory neurons and higher temporal selectivity in the excitatory neurons (Pesavento et al., 2010). This difference between neuronal subclasses may be an essential component of how local synaptic input shapes the population response to transient thalamic input.

Using both the hybrid network and off-line simulations, we find that differences in the intrinsic properties of RS versus FS barrel neurons are crucial for enabling the network to enhance barrel sensitivity to input timing. In addition, changes to the input resistance (leak conductance) of either FS or RS neurons strongly alter the processing ability of the network, consistent with our previous model predictions.

Our hybrid network allows full control over synaptic connections and intrinsic membrane properties, enabling us to explore how they each affect response sensitivity to the number of active thalamic synapses as well as sensitivity to the timing of their input. The results presented here indicate a close inter-relationship between neuron- and network-level processing in determining local circuit function. The differences of individual neuronal membrane properties result in selective responses to input in the absence of local network synapses. The addition of network synapses then additionally increases the selectivity of the neurons. The final step in this reciprocal interaction occurs when the membrane properties of individual neurons are changed, thus altering the effect of the network input on neuronal population output.

## METHODS

We generated a computational model of a barrel network by synaptically connecting RS and FS neurons and construct thalamic spike volleys based on known responses to whisker deflections. Using the

dynamic clamp, we present virtual synaptic conductances from the model neurons and thalamic inputs. Finally, we modified the intrinsic properties of the simulated neurons and observe the results. Many aspects of our simulated network are conceptually based on previous work (Kyriazi and Simons, 1993). Model neurons and simulated networks are constructed probabilistically by varying parameters to generate responses that conform to experimental data at the level of both the barrel network and barrel neurons. Membrane conductance values and individual synaptic strengths are drawn from normal distributions centered on mean values such that simulated neural responses have the same mean and variance as real neurons. Network connections are assigned randomly, but with convergence values in accord with the known connectivity estimates of the barrel cortex network. This strategy ensures that each instance of our simulated and hybrid networks is unique and that our results are robust to heterogeneities (Skinner et al., 2005). At the same time, however, both the neurons and network of each simulation closely approximates real features of barrel circuitry to the extent of our present knowledge.

**Preparation and Electrophysiology**

All electrophysiological methods were performed as reported previously (Pesavento et al., 2010). Whole cell dynamic clamp recordings were taken from layer 4 regular spiking (RS) neurons. Cortical slices 400 μm thick were obtained using a mechanical vibratome (World Precision Instruments, Sarasota, FL) from Sprague-Dawley rats on postnatal day 13-24, using the near-coronal slicing angle described by Land and Kandler (2002). Slices were bathed in artificial cerebrospinal fluid (ACSF) containing (in mM) 126 Na, 3 KCl, 1.25 $NaH_2PO_4$, 2 $MgSO_4$ , 26 $NaHCO_3$, 10 dextrose, and 2 $CaCl_2$, and saturated with 95% $O_2$-5%$CO_2$ at a temperature of 35$^oC$. Borosilicate glass micropipettes were pulled with a Flaming-Brown puller (P97, Sutter Instruments) to a tip resistance of 5-10 MΩ and access resistance of 18-30 MΩ, and were filled with an internal solution consisting of (in mM) 135 K-gluconate, 4 KCL, 2 NaCL, 10 Hepes, 0.2 EGTA, 4 ATP-Mg, 0.3 GTP-Tris, and 7 phosphocreatine-Tris (pH 7.25, 290 mOsm). Whole-cell patch recordings were made in current clamp mode using an Axon Instruments Multiclamp 700B

amplifier. All protocols were reviewed and approved by the University of Rochester Committee on Animal Resources (UCAR).

Barrels were clearly visible in the living slice. Only layer 4 barrel neurons were examined in this study. A small constant holding current (maximum ±100 pA) was applied to bring the neuron's dialyzed resting potential to -65 mV to facilitate comparisons between cells. Previous studies have found that slight modulations of the membrane potential strongly influence the amplitude of post-synaptic potentials, as well as the timing of evoked action potentials (Petersen et al., 2003; Sachdev et al., 2004); here we attempted to minimize those differences by keeping the rest potential consistent within the experiments.

We controlled current injection, data collection, and real-time (i.e. dynamic clamp) stimulation using Labview-RT software (National Instruments) written specifically for the task. A host computer system running custom Labview software controlled stimulus parameters and file I/O. A slave computer system running custom software on the Labview-RT operating system performed all real-time calculations for network simulation and conductances to apply to a single *in vitro* neuron via an A/D converter (National Instruments). Membrane potentials were recorded using an Axon Instruments amplifier, and response waveforms were sampled and digitized at 10 KHz.

We injected square current pulses into each neuron to classify the neuron and quantify several standard response measures. Pulses lasted 1000 ms, ranged in amplitude between ±0.4 nA in 0.1 nA increments, and were presented at a rate of 0.5 Hz. Cells were classified as regular spiking (RS), fast spiking (FS) or low-threshold spiking (LTS) according to previously established criteria (Pesavento *et al.*, 2010; Gibson et al., 1999). Only responses from *in vitro* RS barrel neurons were analyzed in this study. All observed intrinsic membrane properties, such as input resistance and membrane time constant, are similar to those previously reported (Pesavento et al., 2010).

There was little spontaneous activity within the slice (Pesavento et al., 2010). Currents and virtual conductances were applied to a single cell, eliciting at most one or two spikes. Stimulating a single

neuron does not activate the slice network; thus, the results observed are unaffected by other neurons in the slice. Initial studies tested this by pharmacologically blocking synaptic interactions by applying kynurenic acid and picrotoxin to the bathing solution. We observed no change in the single neuron response measures (data not shown).

**Simulated RS and FS neurons**

Single compartment conductance-based models of regular spiking (RS) and fast spiking (FS) neurons were created using current balance equations (Pesavento et al., 2010). To generate a heterogeneous network, we varied the values of each maximal conductance so that the intrinsic membrane properties of the model neurons are within the range of those measured from real barrel neurons recorded *in vitro* (Beierlein et al., Pesavento et al., 2010). Network simulations generated populations of model neurons by randomly selecting the maximum conductances and radius based on a Gaussian distribution with means listed and standard deviation of 5% of the mean. Membrane capacitance density was held constant at 1.0 μF/ $cm^2$ for all neuron classes. All membrane parameters are given in terms of the both the mean channel conductance density and specific conductances; actual values vary about those means.

We modeled conductance-based RS and FS neurons using current-balance equations that describe membrane voltage:

$$C_m \frac{dV_{RS}}{dt} = I_{leak}(V) + I_{Na}(V, \mathrm{h}) + I_{Kdr}(V, n) + I_{AHP}(V, w) + I_{app} + I_{synX}$$

$$C_m \frac{dV_{FS}}{dt} = I_{leak}(V) + I_{Na}(V, \mathrm{h}) + I_{Kdr}(V, n) + I_{D}(V, w) + I_{app} + I_{synX}$$

$$I_{ion} = g_{ion} a^p b^q \left(E_{ion} - V_Y(t)\right)$$

where $C_m$ is the specific membrane capacitance, $V_Y$ is the membrane potential for a neuron of class Y (RS or FS), $I_{ion}$ are ionic currents, $I_{app}$ is the applied current such as a square pulse, and $I_{synX}$ is the simulated synaptic input from presynaptic neuronal population X (E, excitatory; I, inhibitory; T, thalamic). For each ionic current $g_{ion}$, is the maximal conductance, a and b are the proportion of channels

that are activated and deinactivated, respectively, p and q are integers, and $E_{ion}$ is the reversal potential for the given population of ion channels. Currents in the model RS neuron include fast sodium (Na) and potassium currents ($K_{dr}$), an after-hyperpolarization current (AHP), and a passive leak current (leak). Currents in the model FS neuron include fast sodium (Na) and potassium currents ($K_{dr}$), a slowly inactivating potassium current (D), and a passive leak current (leak).

***Model RS neurons***

In simulated RS neurons, the soma is modeled as a sphere with radius=0.0031 cm. The leak conductance is $g_{leak}$=0.057 mS/cm$^2$ (6.883 nS), with a reversal potential of $E_{leak}$=-67 mV.

$$I_{leak}(V) = g_{leak}\,(E_{leak} - V)$$

The fast sodium current is defined as

$$I_{Na}(V,h) = g_{Na}\,m_{\infty}^{3}(V)\,h\,(E_{Na} - V)$$

$$\frac{dh}{dt} = \frac{h_{\infty}(V) - h}{\tau_h(V)}$$

$$m_{\infty}(V) = \frac{1}{1 + \exp\left(-\frac{V-\theta_m}{\sigma_m}\right)}$$

$$h_{\infty}(V) = \frac{1}{1 + \exp\left(-\frac{V-\theta_h}{\sigma_h}\right)}$$

$$\tau_h(V) = 0.37 + 2.78\frac{1}{1 + \exp\left(-\frac{V-\theta_{h\tau}}{\sigma_{h\tau}}\right)}$$

where $g_{Na}$=42 mS/cm$^2$ (5.072 nS), $E_{Na}$=55 mV, and the kinetic equation parameters are $\theta_m$=-20 mV, $\sigma_m$=9.5 mV, $\theta_h$=-40 mV, $\sigma_h$=-7 mV, $\theta_{h\tau}$=-40.5 mV, $\sigma_{h\tau}$=-6 mV. $\theta_m$ was shifted 10 mV to the right along the voltage axis to match the observed *in vitro* spike threshold (Golomb et al 1997). The delayed rectifier potassium current is defined as

$$I_{Kdr}(V,n) = g_{Kdr}\,n^4\,(E_K - V)$$

$$\frac{dn}{dt} = \frac{n_\infty(V) - n}{\tau_n(V)}$$

$$n_\infty(V) = \frac{1}{1 + \exp\left(-\frac{V-\theta_n}{\sigma_n}\right)}$$

$$\tau_n(V) = 0.37 + 1.85\frac{1}{1 + \exp\left(-\frac{V-\theta_{n\tau}}{\sigma_{n\tau}}\right)}$$

where $g_K$=2.2 mS/cm$^2$ (0.266 nS), $E_K$=-90 mV, $\theta_n$=-20 mV, $\sigma_n$=9.5 mV, $\theta_{n\tau}$=-40.5 mV, $\sigma_{n\tau}$=-6 mV. $\theta_n$ is shifted 12 mV to the right along the voltage axis to match the observed *in vitro* spike threshold.

The after-hyperpolarization (AHP) current is a slow $K^+$ current that is responsible for firing rate adaptation in RS neurons, similar to other slow $K^+$ currents used in other models (Pinto et al, 2003; Prescott and Sejnowski, 2008). The form of the equation that we use is based on Pinto et al. (2003) and Kopell et al. (2000):

$$I_{AHP}(V, n) = g_{AHP} w (E_K - V)$$

$$\frac{dw}{dt} = \frac{w_\infty(V) - w}{\tau_w(V)}$$

$$w_\infty(V) = \frac{1}{1 + \exp\left(-\frac{V-\theta_w}{\sigma_w}\right)}$$

$$\tau_w(V) = \frac{800}{3.3\exp\left(\frac{V-\theta_w}{\sigma_{wt}}\right) + \exp\left(\frac{V-\theta_w}{\sigma_{wt}}\right)}$$

where $g_{AHP}$=0.08 mS/cm$^2$ (0.00966 nS), $E_K$=-90 mV, $\theta_w$=-25 mV, $\sigma_w$=10 mV ,$\sigma_{w\tau}$=20 mV. $\theta_w$ is shifted 10 mV to the right along the voltage axis to match the observed *in vitro* spike threshold. The scaling parameter in the numerator of $\tau_w(V)$ has also been changed to give a peak time constant of 22 ms at -37 mV, matching the observed time constant of *in vitro* RS neurons (Pesavento et al., 2010).

***Model FS neurons***

In simulated RS neurons, the soma is modeled as a sphere with radius=0.0019 cm. The leak conductance is $g_{leak}$=0.25 mS/cm$^2$ (11.3 nS), with a reversal potential of $E_{leak}$=-67 mV.

$$I_{leak}(V) = g_{leak}(E_{leak} - V)$$

The fast sodium current is defined as

$$I_{Na}(V,h) = g_{Na}\, m_{\infty}^{3}(V)\, h\, (E_{Na} - V)$$

$$\frac{dh}{dt} = \frac{h_{\infty}(V) - h}{\tau_h(V)}$$

$$m_{\infty}(V) = \frac{1}{1 + \exp\left(-\frac{V-\theta_m}{\sigma_m}\right)}$$

$$h_{\infty}(V) = \frac{1}{1 + \exp\left(-\frac{V-\theta_h}{\sigma_h}\right)}$$

$$\tau_h(V) = 0.5 + 14.0\frac{1}{1 + \exp\left(-\frac{V-\theta_{h\tau}}{\sigma_{h\tau}}\right)}$$

where $g_{Na}$=50 mS/cm$^2$ (2268.2 nS), $E_{Na}$=55 mV, $\theta_m$=-24 mV, $\sigma_m$=11.5 mV, $\theta_h$=-58.3 mV, $\sigma_h$=-6.7 mV, $\theta_{h\tau}$=-60 mV, $\sigma_{h\tau}$=-12 mV. Our value of $\theta_m$ gives simulation results that are in agreement with Golomb et al. (2007) and that closely approximate observed *in vitro* responses of real FS neurons to simulated thalamic input.

The delayed rectifier $K^+$ current $I_{Kdr}$ is based on Kv3.1/2 channels found in FS neurons and is responsible for both their narrow action potential width (Beierlein et al., 2003; Chow et al., 1999) and for their high firing frequency (Erisir et al., 1999; Lien & Jonas, 2003). All parameters are identical to those used in Erisir et al (1999),

$$I_{Kdr}(V,n) = g_{Kdr}\, n^2\, (E_K - V)$$

$$\frac{dn}{dt} = \frac{n_{\infty}(V) - n}{\tau_n(V)}$$

$$n_{\infty}(V) = \frac{1}{1 + \exp\left(-\frac{V-\theta_n}{\sigma_n}\right)}$$

$$\tau_n(V) = \left(0.087 + \frac{11.4}{1 + \exp\left(\frac{V+14.6}{8.6}\right)}\right)\left(0.087 + \frac{11.4}{1 + \exp\left(-\frac{V-1.3}{18.7}\right)}\right)$$

where $g_{Kdr}$=150 mS/cm$^2$ (6804.7 nS), $E_K$=-90 mV, $\theta_n$=-12.4 mV, $\sigma_n$=6.8 mV.

The $I_D$ current is a voltage-dependent $K^+$ current with fast activation and slow inactivation (Storm, 1988; Coetzee et al., 1999; Toledo-Rodriguez et al., 2004), and is dendrotoxin-sensitive. Slowly inactivating Kv1.1 channels have been found in FS cells (Goldberg et al., 2008), and serve to regulate the firing rate of FS neurons in response to near-threshold depolarizations. This channel is distinct from the Kv1.3 channel used by Erisir et al. (1999), which was based on human T-lymphocytes. Parameters were chosen so that our simulated FS neuron responded to square current pulses similar to real FS neurons recorded *in vitro*:

$$I_D(V, a, b) = g_D\, a^3 b\, (E_K - V)$$

$$\frac{da}{dt} = \frac{a_\infty(V) - a}{\tau_a}$$

$$\frac{db}{dt} = \frac{b_\infty(V) - b}{\tau_b}$$

$$a_\infty(V) = \frac{1}{1 + \exp\left(-\frac{V-\theta_a}{\sigma_a}\right)}$$

$$b_\infty(V) = \frac{1}{1 + \exp\left(-\frac{V-\theta_b}{\sigma_b}\right)}$$

where $g_D$=0.15 mS/cm$^2$ (6.805 nS), $E_K$=-90 mV, $\theta_a$=-50 mV, $\sigma_a$=20 mV, $\tau_a$=2 ms, $\theta_b$=-70 mV, $\sigma_b$=60 mV, $\tau_b$=150 ms. The maximum conductance $g_D$ was selected such that the model FS neuron displays classic type-2 dynamics, as we and others have observed *in vitro* (unpublished data; Golomb et al., 2007).

**Changing neuronal leak conductance**

In several experiments, we systematically varied the leak conductance density of the simulated RS and FS neuronal subpopulations ($g_{leak}E$ and $g_{leak}I$, respectively). Simulated RS neurons had a baseline mean leak conductance density ($g_{leak}E$) of 0.057 mS/cm$^2$, and was varied from 0.025-0.12

mS/cm$^2$ (3.02-14.49 nS). Simulated FS neurons had a baseline mean leak conductance density ($g_{leak}I$) of 0.25 mS/cm$^2$, and was varied from 0.05-0.45 mS/cm$^2$ (2.27-20.41 nS). Changing the neuronal leak conductance exhibits an inverse relationship with input resistance and the membrane time constant, as expected from the current-balance equations (Pesavento et al., 2010).

**Simulated inhibitory RS neurons**

A major goal of our study was to explore how differences in the intrinsic properties of RS versus FS neurons influence network processing. To examine this, we made the intrinsic membrane properties of simulated RS and FS neurons to be identical. That is, simulated FS neurons were given the same membrane capacitance, radius, conductances, and channel kinetics as simulated RS neurons. The role in the network of the modified FS neurons was left unchanged, e.g. synaptic convergence, kinetics, and maximum synaptic conductances were kept the same as before (Fig. 1A, right). In the text and figures, we refer to the modified FS neurons as inhibitory RS (RSi) neurons.

**Simulated synapses**

The arrival of a spike onto either real or simulated neurons evokes a synaptic conductance. Simulated synaptic conductances were governed by the following equation: *a(t)*:

$$a(t) = \begin{cases} 0 & t < 0 \\ \left(e^{-\frac{t}{\tau_2}} - e^{-\frac{t}{\tau_1}}\right) & t \geq 0 \end{cases}$$

where thalamic (T) and excitatory (E) synapses were based on AMPA synapses, with time constants $\boldsymbol{\tau_1}$=0.0935 ms, $\boldsymbol{\tau_2}$=1.4286ms, which are related to the rise and fall times of a unitary excitatory post-synaptic current (EPSC), respectively (Hausser and Roth, 1997; Ermentrout, 1998b; Kleppe and Robinson 1999). Inhibitory (I) synapses were based on $GABA_a$ synapses, with time constants $\boldsymbol{\tau_1}$=0.1930ms, $\boldsymbol{\tau_2}$=5.5555 ms for a unitary inhibitory post-synaptic current (IPSC) (Destexhe et al., 1998).

Synaptic currents were generated by summing the scaled conductances from all neurons from subpopulation X, and multiplying it by the driving force for the postsynaptic neuron i:

$$I_{synX}(t) = \left(E_{synX} - V_i(t)\right)\sum_{j=1} gsynX_{ij} \sum_{k=1}^{n} \alpha_j(t - t_{jk})$$

where $gsynX_{ij}$ is the maximum synaptic channel conductance from presynaptic neuron j of type X (thalamic, T; excitatory, E; or inhibitory, I) to postsynaptic neuron i, and the driving force given by the difference of the synaptic reversal potential $E_{synX}$ ($E_{THAL}$=0 mV, $E_{AMPA}$=0 mV, $E_{GABA}$=-80 mV) and the membrane potential $V_i(t)$ of postsynaptic neuron i. The membrane potential of an *in vitro* neuron was obtained in real-time via the conductance clamp. The function $a(t)$was summed at each time step over each spike time $t_{jk}$, which is the time of spike number k from neuron j onto neuron i.

Values for the maximum synaptic conductance $gsynX_{ij}$ were selected to provide a good fit to experimental data examining unitary PSPs onto barrel neurons via paired recordings or minimal current stimulation between thalamic, RS, and FS neurons (Beierlein, 2003; Bruno and Sakmann, 2006). Importantly, these recordings were made at or near the soma, after synaptic PSPs had been shaped by dendritic spatial integration and/or active dendritic processing. Thus our simulations partially capture the effects of dendritic processing on unitary responses. The same synaptic dynamics are used in both simulated and hybrid networks. Figure 1E presents an example voltage trace obtained from an RS neuron generated in response to the current evoked by a single simulated input spike.

To introduce heterogeneity across synapses, we varied each maximum synaptic conductance using a normal distribution with mean $gsynX_{ij}$ and standard deviation of $0.2 * gsynX_{ij}$, or 20% of the mean maximum conductance, resulting in PSPs with amplitude variance similar to those observed *in vitro* (Beierlein et al., 2003). We believe that this is a reasonable first-order approximation for the observed amplitude distribution, which is positively skewed. Due to the transient nature of the thalamic inputs and

cortical responses, we are not including synaptic depression or facilitation in our model. Mean maximum synaptic conductance values are given in Table 1.

It is known that FS neurons in barrel cortex receive stronger thalamic inputs than do RS neurons (Beierlein et al., 2003; Cruikshank et al., 2007). In contrast to our previous study (Pesavento et al., 2010), we scaled thalamic EPSPs onto model FS neurons to an amplitude of 4 mV. The increased EPSP resulted in a thalamic input magnitude threshold (number of spikes) that is 60% of what is observed in RS neurons (9 spikes versus 16, respectively). For all simulated thalamic inputs in this study, we held the ratio of thalamic input magnitude to inhibitory neurons (TI) to be 60% of the thalamic inputs on excitatory neurons (TE); thus as we varied TE, TI was 0.6*TE. FS neurons typically have a higher probability of thalamic convergence than RS neurons (Bruno and Simons, 2002). However, in this study we are not modeling the nonlinear effects of synaptic integration on dendritic arbors, only the PSPs observed at the soma.

Changes in the leak conductance for a given neuron also results in a change to the size and shape of PSPs arising from synaptic conductances. To isolate the effect of intrinsic properties from those of the network, each change in leak conductance was accompanied by a change in the maximum conductance for all arriving synapses so that PSPs retained their original size and approximate shape.

**Simulated thalamic input volleys**

We used the dynamic clamp to generate conductance waveforms that simulate thalamic synaptic input volleys evoked by fast, medium, and slow whisker deflections as described previously (see Fig. 2 in Pesavento et al., 2010). We constructed simulated input spike volleys (Fig. 1D) by modeling real thalamic spike time distributions evoked by fast, medium, and slow velocity caudal whisker deflections, as reported previously (Pesavento et al., 2010; Pinto et al., 2000) (Fig. 1B). Simulated spike times were selected using a family of log-logistic functions known as Fisk distributions (Fisk, 1961) (Fig. 1C).

For each stimulus presentation, a pool of 200 thalamic spike times was generated, approximating the number of thalamic neurons that project to a single barrel (Land et al., 1995; Varga et al, 2002; Bruno and Sakmann, 2006). Thalamic inputs to an individual neuron, simulated or *in vitro*, were applied as a fixed number of spike times (input magnitude) drawn from the pool of 200 spikes. This allows for the possibility that a given thalamic spike may arrive at more than one cortical neuron via thalamocortical divergence. In a simulation with intracortical connections present, 35 excitatory neurons receiving a mean input of 26 thalamic spikes, and 15 inhibitory neurons receiving 16 thalamic spikes, 1150 total thalamic input spikes are required for the simulation. Given that there are 200 spike times available, each thalamic spike will be propagated to about 6 neurons on average, allowing limited synchrony of thalamocortical synapses onto separate neurons.

We quantify thalamic input volleys in terms of timing and magnitude. Input timing is defined as the time required to generate 50% of the total spike count: 2, 5, and 8 ms for fast (F), medium (M), and slow (S) volleys, respectively (Fig.1C). This can also be understood as the median time for the cumulative distribution function (CDF).

Input magnitude is defined as the total number of spikes presented to a single neuron due to a single stimulus. Input magnitude was varied in increments of 3 spikes centered around a threshold value (T) that evoked a single output spike on 50% of all trials using the medium timing distribution. This is consistent with experimental data suggesting that barrel neurons fire sparsely in response to whisker deflections (Brecht and Sakmann, 2002). An increment of 3 spikes roughly corresponds to the 15% change in thalamic input magnitude observed *in vivo* using whisker deflections of different magnitudes (Pesavento et al., 2010; Pinto et al., 2000). For example, if a RS neuron generates a spike half of the time with presentation of 26 spikes, T=26 and the input magnitudes used would be 23, 26, 29, 32, and 35 spikes over each of the input timing distributions. The threshold value T varies with each *in vitro* neuron (Pesavento et al., 2010), therefore we estimate this value prior to running the full data collection. Input threshold is expressed in the normalized units around T throughout all figures.

We assessed the responses of each neuron to input volleys from the three temporal distributions and five different magnitudes, for a total of 15 volleys. Each volley was presented 25 times at a rate of 2 Hz with both the timing and magnitude randomized between trials. A new set of specific thalamic spike times were constructed each time a stimulus was presented, as described above.

**Simulated neuronal network**

Network simulations consisted of 35 RS neurons and 15 FS neurons, thereby maintaining a ratio of 70:30 excitatory to inhibitory neurons in a network with 50 neurons total. The barrel circuit was modeled as a random sparse network. Connections between subpopulations (RS and FS) were determined probabilistically based on estimates from pairwise recordings (Gibson et al., 1999; Beierlein et al., 2003; Sun et al., 2006; Cruikshank et al., 2007). Convergence from one subpopulation to another was defined as the mean probability that one cell will connect to another. Feedforward inhibition (IE) had a default convergence probability of 0.7 (a given inhibitory neuron had a 70% chance of having a single synapse on an excitatory neuron), recurrent excitation (EE) was 0.15, feedforward excitation (EI) was 0.5, and recurrent inhibition (II) was 0.2. These default connectivity values were found to give barrel-like responses (e.g. sensitive to input timing, net damping effect; c.f. Fig.3) and conform to connection probabilities determined experimentally using paired recordings. Convergence values were also varied systematically as described in the results. Synaptic conductances were constructed as described above.

**Hybrid network**

Hybrid networks were constructed by using the dynamic clamp to mediate real-time interactions between real and simulated barrel neurons. In effect, we removed one of the simulated RS neurons from a 50 neuron network simulation and inserted a biological RS neuron from the *in vitro* slice recording in its place (Fig. 1A).

Spike times from the real RS neuron were taken to be at the peak of recorded action potentials, and were passed to the simulated neurons to generate simulated synaptic conductances as described

below. Spikes in simulated RS or FS neurons that were connected to the real neuron evoked synaptic conductances scaled to match excitatory or inhibitory post-synaptic potential (EPSP or IPSP) amplitudes and variability as described below, and applied to the *in vitro* RS neuron using the dynamic clamp with an update rate of 10 kHz.

**Individual neuron response measures**

For each network condition, we assessed the responses of each neuron to input volleys across the three timing distributions (fast (F), medium (M), and slow (S)) each having 5 different magnitudes for a total of 15 volleys. We quantified responses of individual neurons in terms of response threshold, latency, and variability. Response threshold was defined as the minimum number of input spikes required to evoke an output spike within 50 ms of stimulus onset on 50% of the trials. We obtained the response threshold by fitting a linear regression over spike generation probabilities between 10% and 90% in response to the medium time distribution, and interpolated to find the number of spikes that would generate a response with a probability of 50%. We define response latency as the time to first spike after stimulus onset, measured at time of the peak of the first action potential. We define response variability as the standard deviation of latency measured over 25 trials using the same thalamic input volley parameters but with new thalamic spike times.

We quantified the sensitivity of each response measure (threshold, latency, variability) to each input parameter (timing, magnitude) using multivariate linear regression analysis on a cell by cell basis (Matlab Statistics Toolbox). The sensitivity of response threshold to input timing was quantified as the slope of the regression line relating the two. The sensitivity of response latency to input timing was quantified as the slope of the regression plane measured along the input timing axis. The sensitivity of latency to input magnitude was quantified as the absolute value of the slope of the plane measured along the input magnitude axis. The sensitivity of response variability to input timing and magnitude was measured the same way.

**Excitatory population response measures**

Population measures focused on the RS population since these represent the output of the layer 4 barrel circuit. Population measures were quantified in terms of spikes per stimulus per neuron in a 50 ms window following the arrival of the simulated thalamic volley. Population measures from real neurons were constructed by combining responses from all neurons using the same stimulus conditions; each stimulus condition was applied 25 times. Population measures from simulated neurons were constructed by combining responses from the 35 simulated neurons in the network over 25 repetitions of each stimulus condition.

The sensitivity of population responses to input timing and magnitude was quantified as the absolute values of the two corresponding slopes of the regression plane fit to the excitatory activity (spikes/stimulus) over the input timing (F=2 ms, M=5 ms, S=8 ms) and input magnitudes T, T+3, and T+6. T-3 is included in figures for a subthreshold comparison, and is not included in the regression analysis.

All *in vivo* data are taken from previously published results (Pinto et al., 2000).

**Randomization of network properties**

For each stimulus presentation, simulated neurons and networks were constructed probabilistically by varying parameters to generate responses that conform to experimental data at the level of both the barrel network and barrel neurons. Membrane conductance values and individual synaptic strengths are drawn from normal distributions centered on mean values such that simulated individual neural responses have the same mean and variance as real neurons. Network connections were assigned randomly, but with convergence values in accord with the known connectivity estimates of the barrel cortex network. In effect, a new set of barrel neurons and a barrel-like network was randomly constructed for each instance of the simulation. This strategy ensures that each instance of our simulated and hybrid networks is unique and that our results are robust to heterogeneities (Skinner et al., 2005). At

429 the same time, however, both the neurons and network of each simulation closely approximates real
430 features of barrel circuitry to the extent of our present knowledge.

431 **Software and statistics**

432 Our network simulation software was written using C++ and compiled into a dynamically shared
433 library that was used in offline network simulations in Matlab as well as the real-time hybrid network
434 simulations within the dynamic clamp using Labview. Importantly, simulated and hybrid networks as
435 well as the dynamic clamp interface used the same library to simulate neurons, networks, and
436 conductances. The dynamic clamp was implemented on a custom-built PC with an Intel Core 2 Duo
437 E6850 that was stably overclocked to 3.4 GHz. This allowed us to simulate up to 200 neurons (up to 5
438 differential equations each) in real-time with 10 kHz sample rate. However, the stability of real-time
439 interactions decreased with more network connections and/or spiking activity. Thus, we used networks of
440 50 neurons so that stability could be maintained for all network conditions we examined. Numerical
441 integration was with $4^{th}$ order Runge-Kutta with a 100 μs integration step size, matching the 10 kHz
442 sample rate of the dynamic clamp.

443

## RESULTS

### Hybrid network enhances differences between input conductance timing distributions

Utilizing the dynamic clamp to apply simulated synaptic conductances to layer 4 RS neurons *in vitro*, we first examine the summed conductance in response to thalamic input (Fig. 1F) or thalamic input as well as synaptic input from the simulated barrel network (Fig. 1G). We define the total synaptic conductance onto a single RS neuron as the sum of each individual synaptic conductance from thalamic, excitatory, and inhibitory synapses from the simulated network: $G_{syn} = g_{thal} + g_E + g_I$. We also consider the effective synaptic reversal potential: $\hat{E}_{syn} = (g_{thal}E_{AMPA} + g_E E_{AMPA} + g_I E_{GABA})/G_{syn}$ (Fig. 1H). Note that both quantities vary over time and depend on activity in the hybrid network.

When the neuron is acting without the hybrid network (Fig.1F), the total synaptic conductance is due solely to thalamic input. Both the rate of rise and the peak magnitude depend on the timing of the input volley. The cumulative sum of synaptic conductance (i.e. the area under each curve) is consistent across all input timing distributions. Because of the lack of inhibition, the synaptic reversal potential is constant, resulting in a constant depolarizing synaptic drive to the subthreshold membrane potential (Fig. 1H, left).

In the presence of the hybrid network, the total synaptic conductance is shaped by the combination of thalamic input as well as local excitatory and inhibitory synapses. Importantly, neurons in the barrel-like hybrid network require more thalamic input to reach threshold compared to neurons acting without the network. Because the simulation parameters were set so that the cell spiked, the total synaptic conductance is larger, resulting in a bigger difference in both the rate of rise and in the peak conductance magnitude between fast and slow inputs (Fig. 1F).

The presence of late inhibition further increases the synaptic conductance, as well as rapidly hyperpolarizing the synaptic reversal potential just after the thalamic conductance reaches its maximum (Fig. 1H, right). Excitatory synapses from recurrent excitation have little effect on the late component of

the net conductance waveform, but serve to slightly depolarize the late component (>5 ms for fast inputs, >10 for slow inputs) of the synaptic reversal potential. Interestingly, since fast stimuli evoke stronger inhibition (Pesavento et al., 2010), the changes in driving force occur earlier for fast inputs (Fig. 1H). This effectively shortens the duration in which rapid thalamic input can generate an action potential in excitatory neurons, which in turn requires more thalamic input to reliably generate a response. Thus, fast inputs will generate responses that occur more reliably and with shorter latency than slow inputs in the presence of network connections.

**Individual neuron responses to hybrid network input**

We examined the responses of 39 RS barrel neurons recorded *in vitro* in response to simulated thalamic input, with and without the presence of simulated barrel network connections via the hybrid network. Figure 2 shows example traces and measures from an example *in vitro* RS neuron in response to three timing distributions of thalamic input at the threshold input magnitude T. In the presence of the hybrid network, spikes occur earlier and with less variability than with thalamic input alone (Fig. 2A). The same neuron required more thalamic input to reach threshold T in the presence of network connections versus the absence (24 versus 15 input spikes, respectively). When embedded in the network, the input threshold is less sensitive to changes of input magnitude and more sensitive to changes of input timing (Fig. 2B). Moreover, both the spike latency (Fig. 2C) and spike variability (Fig. 2D) decrease in the presence of network connections.

We compiled similar data from 39 *in vitro* RS neurons and 35 simulated RS neurons both while isolated and while embedded in a hybrid network (Table 1). In the presence of network connections, the mean threshold and threshold sensitivity to input timing are significantly higher than in with thalamic input alone. The unexpectedly lower threshold sensitivity to timing in the simulated neuron can be explained by the lack of dendrites in the computational model. The sharp rise of sensitivity in the real neuron compared to the simulated neuron is likely due to dendritic shunting, in which a slow current

applied at the soma has a greater propensity to be shunted by the dendrites then a fast input would. Our simulated neurons do not have dendrites, so would not experience this shunting effect. Latency, variability, and the sensitivities of each to input timing and input magnitude are reduced in the presence of network connections. All changes of response measures are similar between *in vitro* and simulated RS neurons.

Taken together, our results suggest that neurons embedded in barrel circuits require more thalamic input to reach threshold, but fire earlier and with less variability than neurons acting alone. In all of our measures, with the exception of the previously noted threshold sensitivity to input timing, the effect of network connections on the responses of both real and simulated neurons of the hybrid network was the same (Table 1).

**Population response of connected versus individual excitatory barrel neurons**

One of the primary goals of this study is to examine how the presence of local excitatory and inhibitory input alters the population response to transient thalamic input. We combine the responses from the same 39 *in vitro* RS neurons to the different simulated thalamic inputs in the presence or absence of hybrid network connections. The additional transient synaptic conductances significantly altered the ensemble response to different input conditions.

Population spike density histograms, showing the pooled spike times from 39 RS neurons *in vitro*, indicate the temporal distributions of responses to simulated thalamic input. Responses for each neuron are aligned to input threshold (T) (Fig. 3A-B). When acting within the hybrid network (thalamic + network input), *in vitro* population responses are less temporally distributed but are more sensitive to input timing (compare rows) and less sensitive to input magnitude (compare columns) then when acting individually (thalamic input only). Hybrid network responses are similar to responses observed *in vivo* (Pinto et al., 2000), specifically in the difference of response magnitude across input timing (Fig. 3C). However, the *in vivo* responses have a broader temporal distribution than those observed with the *in vitro*

516 hybrid network responses. Despite the temporal difference, it is likely that the downstream neurons
517 integrate the responses from layer 4 RS neurons, indicating the importance of spike count across the
518 population.

519 As described in Methods, we quantify RS neuron population responses as spikes per stimulus for
520 the different simulated synaptic input conditions (Fig. 3D-F). In the absence of network connections,
521 excitatory RS neurons are sensitive to both input magnitude (the distance between lines for responses
522 across magnitudes) and input timing (the slopes of the lines) (Fig. 3D), consistent with our previous
523 findings for individual neurons (Pesavento et al., 2010). In the presence of network connections, RS
524 excitatory responses are less sensitive to input magnitude but more sensitive to input timing (Fig. 3E).

525 A comparison of the hybrid network population responses and the *in vivo* responses show many
526 similarities, in particular high sensitivity to input timing and low sensitivity to input magnitude. In our
527 data, the *in vivo* neurons typically generate up to two spikes per stimulus, compared to the *in vitro* one
528 spike per stimulus. This may be a result of the lack of spatial interactions by applying simulated
529 conductances directly to the soma *in vitro*, as opposed to the dendritic arbor as happens naturally *in vivo*.
530 In particular, the soma will be refractory after the initial spike, while charge from the dendritic inputs
531 would continue to facilitate a second spike within the *in vivo* network. This would also explain the wider
532 temporal profile with the *in vivo* spike density histogram (Fig. 3C). It is also important to note that some
533 studies have found more sparse spiking responses to whisker deflections *in vivo* (de Kock et al., 2007;
534 Brecht and Sakmann, 2002). Many of those observed differences of *in vivo* spike count can be attributed
535 to differences in whisker stimulation.

536 Population sensitivity measures elucidate how changes of input conditions, such as timing and
537 magnitude, affect the excitatory population response. The presence of the hybrid network significantly
538 increases the population sensitivity to different input timing distributions ($p<0.001$) (Fig 3G) and
539 significantly decreases the sensitivity to input magnitude ($p<0.001$) (Fig 3H). Both of these measures are

comparable to the sensitivity measures calculated from excitatory neuron responses *in vivo*. In addition, we also found that neurons embedded in networks require more thalamic input to reach threshold (Fig. 3I). This is consistent with the known damping properties of barrel circuitry (Pinto et al., 2003). Taken together, these data suggest the sufficiency of network interactions in shaping the local network response to thalamic input.

**Effect of connectivity on population response sensitivity**

Next, we examined the effect of synaptic convergence on population response sensitivity. We combined the responses of 10 *in vitro* RS neurons while varying the convergence probabilities of feedforward inhibition and recurrent excitation in the hybrid network. Our data suggest that the increased sensitivity to timing in ensemble responses depends mainly on feedforward inhibition (IE); recurrent excitation with relatively low convergence probabilities has little effect on sensitivity to timing (Fig. 4). However, decreased sensitivity to magnitude depends on the balance of both recurrent excitation and feedforward inhibition. Due to the time required to obtain data from multiple network connectivity patterns while holding a cell *in vitro*, we restricted the hybrid networks to no local connectivity (thalamic input only), and four combinations of feedforward inhibition and recurrent excitation: normal IE (0.7), weak IE (0.3), normal EE (0.15), and strong EE (0.5).

When IE is decreased from “normal” to “weak”, the population responses are less sensitive to the timing of thalamic inputs and are more sensitive to input magnitude (Fig. 4B-C). Increasing the strength of recurrent excitation in both the normal and weak IE networks shows little effect on the sensitivity to timing, but has significant effect on the sensitivity to input magnitude (Fig. 4D-E). We quantified response sensitivity as the slope of the line of best fit through the data, and we confirmed that increasing the EE convergence has no effect on the population response sensitivity to input timing (Fig. 4F, hatched versus open bars), while increases the sensitivity to magnitude for both normal and weak IE networks

(Fig. 4G). Importantly, high convergence of feedforward inhibition is sufficient to enhance network selectivity to fast versus slow thalamic inputs (Fig. 4F, white versus gray bars).

**Network connectivity in simulated networks**

While the hybrid network allows us to examine the effect of different network configurations on the response properties of real barrel neurons, the number of networks we can explore is limited by how long we can hold each cell. Therefore, to more thoroughly explore the effect of network connectivity, we examined purely simulated networks over a broad range of values for both feedforward inhibition convergence (IE) and recurrent excitation convergence (EE) values.

Figure 5A-B compares the population responses of simulated RS neurons acting alone (thalamic input) versus synaptically connected (thalamic + network input). As with the *in vitro* neurons (c.f. Fig. 3D-E), network connections result in population responses that are more sensitive to thalamic input timing and less sensitive to input magnitude.

To understand the specific effects of different convergence probabilities, we change the convergence probability of one class of connections while holding the others constant within the simulated network. While holding recurrent excitation constant at barrel-like levels (see Methods), the sensitivity to thalamic input timing increases as the convergence probability of inhibitory to excitatory synapses (IE) increases (Fig. 5C, black). The simulated RS neuron population shows slightly lower sensitivity than the *in vitro* population responses (Fig. 5C, red). Increasing IE also results in a decrease of sensitivity to thalamic input magnitude (Fig. 5E). While holding feedforward inhibition constant, increasing the strength of recurrent excitation has little effect on the population sensitivity to input timing (Fig. 5D); again, there is a notable decrease in sensitivity to timing in the simulated population response compared to the *in vitro* population. Increasing recurrent excitation significantly increases the sensitivity to input magnitude (Fig. 5F). We show the sensitivity to input timing and input magnitude over the full range of convergence probabilities (Fig 5G,H). The sensitivity to timing is almost bowl shaped, with a

high sensitivity with high EE and IE convergence probabilities, with the IE convergence dominating the overall shape of the surface (Fig. 5G). The sensitivity to input magnitude is predictably high for high EE and low IE, and falls off as EE decreases or IE increases (Fig 5H).

**Network damping**

Previous studies have examined the role of strong intracortical inhibition in rendering a net suppressive or *damping* effect on layer 4 barrel responses to thalamic input (Gabernet et al., 2005; Wilent and Contreras, 2004; Pinto et al., 2003). Moreover, theoretical models have shown that damping circuits are selectively responsive to fast inputs (Pinto et al., 2003). The methods used in the present study allow a more detailed investigation of the role of network damping on thalamocortical response sensitivity.

We define *network gain* as the mean excitatory population response in the presence of network connections divided by the mean excitatory population response without network connections. Values less than one indicate that the overall effect of connectivity is inhibitory, or damping, while values greater than one indicate that the overall effect is excitatory or amplifying.

Consistent with previously published results using reduced models (Pinto et al., 2003), we find that damping networks exhibit responses that are more sensitive to timing and less sensitive to magnitude than networks that are amplifying. We show the response sensitivities of a representative damping network and amplifying network. In the presence of network connections the damping network is significantly more sensitive to input timing than the amplifying network (Fig. 6A). The damping network also exhibits a significantly reduced sensitivity to input magnitude, while the amplifying network shows a significant increase of sensitivity to input magnitude (Fig 6B).

To describe the effect of the network on the response sensitivity to input timing or magnitude, we define *network sensitivity gain* as the ratio of sensitivity to input timing or magnitude with the network on divided by the sensitivity with the network off. A network sensitivity gain equal to one indicates that the presence of network connections has no effect on response sensitivity to input conditions. We examined

611 the effect of network gain on network sensitivity gain by changing the IE and EE convergence
612 probabilities (IE=0.1 to1.0; EE=0.05 to 0.75) and thus systematically varying network gain. Simulated
613 thalamic inputs were presented as before, and we recorded the network sensitivity gain of the subsequent
614 responses. Thus, we can compare the functional effect of the network (damping versus amplifying)
615 against the effect of the network in altering the sensitivity to input conditions.

616 We found that nearly all damping networks are more sensitive to the timing of transient synaptic
617 inputs, while amplifying networks are more sensitive to the number of inputs received (Fig. 6C).
618 Networks with low network gain (damping) exhibit high sensitivity to timing and low sensitivity to
619 magnitude, regardless of the specific network configuration giving rise to the network gain. Conversely,
620 amplifying networks exhibit high sensitivity to input timing and magnitude.

621 The relationship between response sensitivity and network function (damping versus amplifying)
622 appears to be robust across a broad range of network convergence values. Observations of response
623 sensitivity to both input timing and magnitude can serve as a way to determine the effect of network
624 connections experimentally. For example, high values of both sensitivity to timing and magnitude may
625 indicate an amplifying network, while high sensitivity to timing and low sensitivity to magnitude
626 indicates that the network is predominantly inhibitory, or damping. Importantly, these results give a
627 valuable insight for understanding the functional role of network connectivity – described as sensitivity to
628 input timing, input magnitude, or a combination thereof – that is independent of specific synaptic
629 convergence values.

630

631 **Neuronal and network responses with inhibitory RS neurons**

632 How much of the effect of the network relies on the difference of intrinsic membrane properties
633 between RS and FS neurons? We create a network of 35 simulated RS and 15 simulated FS neurons (RS-
634 FS network) and present it with simulated thalamic inputs in the presence or absence of local synaptic

connections. Previous results have found that in the absence of synaptic inputs from the local network, RS and FS neurons exhibit different input thresholds, latencies, and variability, resulting from their having different intrinsic membrane properties (Pesavento et al., 2010). In a different set of simulations, we replace all FS neurons in the model with RS neurons while retaining their inhibitory synapses, yielding inhibitory RS (RSi) neurons, i.e., a RS-RSi network. Thus, all neurons in the network have identical intrinsic membrane properties but different network-level effects. Here, we show that differences in the intrinsic properties of FS vs RS neurons are crucial for enhancing the network's sensitivity to input timing. This is illustrated with example networks in Figure 7.

The presence of fast inhibition increases the thalamic input threshold; the increased number of input spikes results in reduced temporal variability across both populations. In a simulated RS-FS network, FS neurons spike approximately 5 ms prior to RS neuron responses in both the absence and presence of network connections (Fig. 7A). In the RS-RSi network, inhibitory neurons respond concurrently with the excitatory neurons both in the absence and presence of network connections; this remains consistent for all thalamic input timing distributions (Fig. 7F). RSi neurons exhibit a slight increase of spike probability later in time, suggesting that these late responses are enhanced by disynaptic feedforward excitation from the RS neurons (Fig. 7F, right).Thus, the input threshold of excitatory RS neurons is slightly higher with than without network input. Because of the transient nature of the stimuli used, these later interactions have no effect on initial RS neuron responses.

Again we utilize the total synaptic conductance envelopes to visualize the timing of each class of input received, as well as estimated synaptic reversal potential as before (c.f. Fig. 1G,H). In the RS-FS network, thalamic synapses ($g_{thal}$) generate the initial rapid increase of conductance, with inhibition ($g_I$) peaking within 5 ms for fast inputs (Fig. 7B). Strong and rapid inhibition immediately but incompletely hyperpolarizes the effective synaptic reversal potential ($\hat{E}_{syn}$) (Fig. 7C). Recurrent excitatory conductances slow membrane hyperpolarization, but more preferentially to fast versus slow inputs (Fig. 7D, arrow). In the RS-RSi network, thalamic inputs are solely responsible for the initial conductance,

660 with inhibition peaking approximately 10 ms after stimulus initiation for fast thalamic inputs (Fig. 7G),
661 much later than inhibition in the RS-FS network (cf. Fig. 7B). In comparison to the RS-FS network,
662 $\hat{E}_{syn}$ of an excitatory neuron in the RS-RSi network remains depolarized for longer, and is rapidly
663 hyperpolarized to the GABA reversal potential (-80 mV) for all three thalamic input timings (Fig. 7H).

664 The inhibitory neurons in the network exhibit different synaptic conductances than the excitatory,
665 with the difference of synaptic convergence readily obvious. Inhibitory FS neurons in our barrel-like
666 network receive feedforward excitatory input (EI) with 0.5 convergence probability, and recurrent
667 inhibitory input with 0.2 convergence probability, as in the Methods. Strong thalamic input is enhanced
668 in duration by feedforward excitation (Fig. 7G). It is clear that the excitatory input from RS neurons is
669 highly dependent on the timing of thalamic input, with high amplitude and duration excitatory
670 conductance in response to fast thalamic inputs, and very little response to slow inputs. Because FS
671 neurons respond early, the recurrent inhibition occurs prior to the start of feedforward excitation for all
672 thalamic input timing. The estimated synaptic reversal potential for FS neurons exhibits a initially
673 depolarizing drive, followed by hyperpolarization from recurrent inhibition (Fig. 7E). The third wave of
674 synaptic conductance is from the slow excitatory neurons, keeping the driving force depolarized. The
675 relative amount of time depolarized varies between different thalamic input timing distributions, more so
676 than with RS neurons (eg Fig 7D). From these results, it is apparent that RS and FS neurons receive
677 different inputs in context of the connected network. The second half of this study aims to identify the
678 role of membrane properties in shaping connected population responses to thalamic input.

679 To examine the effects of identical intrinsic membrane properties in modulating population
680 responses, we utilize the hybrid network and embed *in vitro* RS neurons into both the RS-FS and RS-RSi
681 networks. Figure 8 presents data from 10 *in vitro* RS neurons, showing their pooled responses to both
682 network conditions. As observed previously (cf. Fig 3), population responses of *in vitro* neurons in the
683 presence of hybrid network virtual synapses are more sensitive to input timing and less sensitive to input
684 magnitude than with the connections off (Fig 8A,B). The calculated values of sensitivity to input timing

685 and input magnitude are shown in Figs. 8E and 8F (FS), respectively. In contrast, networks with RSi
686 neurons in place of FS neurons do not show notable change between networks with or without
687 connections (Fig. 8C,D). The sensitivity to input timing in RSi networks increases slightly when
688 connectivity is added (Fig 8E, RSi, not significant), but this change is significantly lower than that
689 observed in FS networks (Fig 8E). RSi networks exhibit a slight decrease in sensitivity to input magnitude
690 (Fig. 8F, RSi). This decrease in sensitivity to input magnitude is not significantly different from FS
691 networks, suggesting the importance of the properties of RS neurons in network processing.

692 It is clear that by removing the differential effects of FS neuron single cell properties, the
693 processing of the network is significantly altered. However, the changes were not consistent across each
694 measure, suggesting different roles of the membrane properties between RS and FS neurons. Next, we
695 examine how changes in input resistance and membrane time constant, altered directly via the passive
696 leak conductance, affects population input sensitivity.

697 **Effect of neuronal leak conductance on network-level processing**

698 RS and FS neurons differ in a number of membrane properties. Our previous work suggests that
699 the difference of input resistance is particularly important to account for differences in their responses to
700 thalamic input (Pesavento et al., 2010). Here, we examine how changes in input resistance in both
701 populations affect network level processing. Note that in our computational models, changes of input
702 resistance are induced by varying the maximum leak conductance. All other membrane parameters are
703 held constant, while maximum synaptic conductances ($g_{syn}$) are scaled to maintain the same PSP
704 amplitude as in the canonical models.

705 We examine the responses of 11 RS barrel neurons embedded in hybrid barrel networks while
706 systematically varying the leak conductance of both the excitatory RS and inhibitory FS neurons in the
707 simulated network (Fig. 9). Our results demonstrate that the effect of network interactions depends
708 strongly on the leak conductance of inhibitory neurons and only marginally on the leak conductance of

709 excitatory neurons. As discussed previously, network connections under normal conditions enhance
710 response sensitivity to input timing and decrease sensitivity to magnitude (compare Fig. 9A, B).
711 Decreasing the leak conductance in the excitatory RS neurons (gleakE) has little effect on the role of the
712 network (compare Fig. 9B, C). However, if we also increase the leak conductance in the inhibitory
713 neurons (gleakI), the enhancement of response sensitivity due to network connections is lost (compare
714 Fig. 9C, D).

715 We compare the sensitivity to timing and sensitivity to magnitude of *in vitro* RS neurons across a
716 subset of networked population leak conductance conditions and the baseline condition without network
717 connections. The number of conditions examined was limited by how long we could reliably hold each
718 neuron using whole cell patch. Nonetheless, the gleakE and gleakI conditions we examined exhibit
719 complex interactions in their effects on population sensitivity to input timing. While decreasing gleakE
720 alone has little effect on the sensitivity to input timing, the addition of high gleakI decreases response
721 sensitivity to input timing, substantially lower than responses in the absence of network connections (Fig.
722 9E). This combination of membrane conductances negates the influence of the network, decreasing the
723 population sensitivity to input timing. In addition, high values of gleakE with low gleakI enhance RS
724 neuron sensitivity to timing (Fig 9E, far right bar). Sensitivity to magnitude is less affected by the
725 differences of leak conductance between the neuronal subpopulations (Fig 9F). Decreasing gleakE
726 slightly increases the sensitivity to input magnitude, regardless of inhibitory leak conductance (Fig. 9F,
727 light gray bars). Note that these effects are after adjusting the synaptic conductances to maintain the same
728 PSP amplitude as used in the null (o) condition; the effects observed are not a direct result of synapse
729 efficacy.

730 These results indicate that the network's sensitivity to input timing depends in part on the fact the
731 input resistance of inhibitory neurons is lower than that of excitatory neurons.

732 **Network sensitivity gain**

While the hybrid network allowed us to examine the effect of different networks on the response properties of real barrel neurons, the number of networks we were able to explore was limited by how long we could hold each cell. Therefore, to examine the effect of neuronal leak conductances more thoroughly, we used simulated networks having a broad range of values for leak conductance in excitatory (gleakE) and inhibitory (gleakI) neurons. Our simulated results indicate that both gleakE and gleakI alter the effect of the network on response sensitivity (Fig. 10). Increasing values of gleakI decrease the effect of the network on sensitivity to input timing; predictably, changing gleakI has no effect on excitatory population responses in the absence of network connections (Fig. 10A). Increasing values of gleakE increase the sensitivity to input timing both in the presence and absence of the network (Fig. 10B).

To quantify better how intrinsic properties influence the role of the network, we define a measure of *network sensitivity gain* as the ratio of the response sensitivity (to timing or magnitude) when the network is present divided by the response sensitivity when the network is absent. A network sensitivity gain of 1 indicates that the presence of the network has no effect on the response sensitivity; a gain less than 1 indicates that network reduces response sensitivity and a gain greater than one indicates that the network increases response sensitivity. Network sensitivity gain to input timing depends strongly on the leak conductance of inhibitory neurons but only weakly on the leak conductance of excitatory neurons (Fig 10C-D). By measuring the regression line and testing whether the slope is significantly different from zero, we found that increasing the inhibitory leak conductance significantly reduces the network sensitivity gain to input timing in simulated RS neurons ($p<1e-4$) (Fig. 10C). Increasing the excitatory leak conductance weakly reduces network sensitivity gain ($p<0.01$) (Fig. 10D). By contrast, the network sensitivity gain to input magnitude is modified by changes of gleakE but not gleakI. Increasing inhibitory leak conductances has no significant effect on network sensitivity gain to input magnitude ($p>0.05$) (Fig. 10E). However, increasing excitatory leak conductances serves to significantly decrease the network sensitivity gain to magnitude ($p<1e-4$) (Fig. 10F).These results suggest separate roles of excitatory and

758 inhibitory subpopulation excitability in shaping the response selectivity to thalamic input, as modulated
759 by leak conductance.

760 Why is the leak conductance of inhibitory neurons a critical parameter in altering the excitatory
761 network sensitivity gain to input timing? To answer this, we examined model RS and FS neuron single
762 cell response measures of s in order to distinguish changes in threshold, latency, or variability across
763 changes of inhibitory leak conductance across the simulated barrel network (Fig. 11). Changing gleakI
764 has no effect on RS neurons in the absence of network connections; therefore we only show the data for
765 RS neurons in the presence of network connections (Fig 11, top row). High leak conductance FS neurons
766 exhibit an increase of spike threshold in both the absence (net off) and presence (net on) of network
767 connections (Fig. 11D). Across increasing gleakI, surprisingly we did not observe changes of spike
768 latency (Fig. 11E), but spike variability showed substantial changes with both network off and on. The FS
769 variability graphs have been separated for visual clarity. With the network off, increasing gleakI results in
770 a decrease of FS neuron spike variability, particularly in response to slow inputs (Fig. 11G). In contrast,
771 the presence of network connections results in an increase of spike variability as gleakI increases (Fig.
772 11F). This may occur as a result of feedback inhibition from early FS neuronal responses increasing the
773 variability of membrane conductance and thus broaden the distribution of spike times without altering the
774 mean latency.

775 Inhibition from high leak conductance FS neurons effectively decreases the spike threshold in RS
776 neurons, decreasing the threshold sensitivity to timing (the distance between the different input timing
777 lines) primarily through a substantial decrease of threshold for slow inputs (Fig. 11A). Notably, this
778 decrease occurs concomitantly with an increase of FS response variability. RS response latency and
779 variability remain unchanged for increasing values of inhibitory leak conductance (Fig. 11B,C). It is clear
780 that changing gleak on FS neurons exhibits complex actions on single cell and population responses of
781 RS neurons.

782

## DISCUSSION

Using a conductance clamp, we embedded *in vitro* RS neurons within a simulated barrel-like network. This hybrid network gives unique opportunity to control the timing and magnitude of synaptic inputs seen by the neuron's soma. This allows the experimenter a unique chance to explore how the presence of simulated network input alters the response properties of neuronal subpopulations to different input, neuronal, and network conditions. By creating a biologically plausible, heterogeneous network simulation and applying its synaptic output to *in vitro* neurons, we demonstrate the effectiveness of barrel-like conditions at enhancing selectivity to input timing. We defined the sensitivity to input timing as the change of population response magnitude (spikes per stimulus) as the median of the thalamic input latency increases. We defined the sensitivity to input magnitude as the change of population response magnitude as the number of active thalamic synapses increases. These metrics quantify how the network excitatory output transforms transient input. We then examine the effects of local network connectivity, dependence on the differences between neuronal subclass membrane properties, and how leak conductance can modulate the effects of network connectivity.

Studies that examined the anatomical and electrophysiological characteristics of barrel neurons (McCormick et al., 1985; Pesavento et al., 2010) as well as their synapses and connectivity (Gibson et al., 1999; Beierlein et al., 2003) allow us to constrain neuronal and network simulations with known biological values and variability, adding to the robustness of our findings. Importantly, the synaptic parameters (e.g. PSP amplitude) were not tuned to give population responses that accurately represent those observed *in vivo*; nonetheless, our results closely approximate known response measures from anesthetized animals (cf. Fig. 3G-H; Pinto et al., 2000). By matching observed single cell responses (Pesavento et al., 2010) and adding network connectivity, we were able to take significant steps forward in understanding the mechanisms that underlie the selectivity of population responses in the *in vivo* animal.

807

808 *Barrel-like connectivity enhances temporal selecitivity*

809 Embedding *in vitro* RS neurons in the barrel-like hybrid network enhances the response
810 selectivity to fast versus slow inputs. When responding to transient thalamic input in context of the
811 network, neurons have a higher probability of generating an action potential in response to fast temporally
812 correlated inputs than when the neuron receives only thalamic input (Fig 2B, Fig. 3D-E). Strong
813 feedforward inhibition is sufficient to enhance the sensitivity to input timing (Fig.4F), while
814 simultaneously decreasing the sensitivity to the number input magnitude (Fig. 4G). Governed by synaptic
815 convergence between neuronal subtypes, the balance of excitation and inhibition can modify the
816 processing modality of the cortical circuit. However, different network connectivity patterns give rise to
817 identical functional effects (e.g. damping, sensitive to input timing) independent of the specific synaptic
818 connectivity (Fig. 6C). Thus, the synaptic convergence probabilities between neuronal subtypes can
819 determine the temporal selectivity and magnitude selectivity within the thalamocortical transformation.

820 The interplay between required thalamic input magnitude and the timing of thalamic and local
821 network input in generating a single action potential is complex, overlying synaptic and cellular
822 mechanisms that directly and indirectly modulate response probability. In order to overcome the effects of
823 feedforward inhibition, more thalamic input is required to generate the same probability of output spike
824 generation. In turn, this enhances the differences of responses to fast, medium, and slow thalamic inputs
825 at the level of single neurons; specifically, the rate of total conductance rise of fast inputs is faster and
826 earlier than that of slow inputs with identical input magnitude (Fig. 1F-G). Feedforward inhibition
827 additionally sharpens these differences by rapidly hyperpolarizing the synaptic reversal potential and
828 correspondingly decreasing the synaptic driving force (Fig. 1H). Recurrent excitatory input begins just
829 after the inhibitory input, serving to slow the rapid hyperpolarization of synaptic reversal potential. These
830 dynamics rely heavily on the relative timing of synaptic input from FS, RS, and thalamic neurons. FS

neurons respond earlier than RS neurons (Pesavento et al., 2010) and, consequently, feedforward inhibition almost always precedes recurrent excitation.

Across all convergence values examined, we find that response sensitivity to input timing depends primarily on feedforward inhibition; recurrent excitation has little effect so long as the network has a net inhibitory effect. As EE increases beyond this threshold, the balance of excitation and inhibition is shifted to a positive feedback regime. The sensitivity of responses to both input magnitude and input timing both increase dramatically and/or the network exhibits unstable epileptiform activity in response to transient thalamic inputs (c.f. Fig. 5H). The sensitivity to input magnitude sharply increases as the strength of recurrent excitation increases and feedforward inhibition decreases, amplifying the strong excitatory thalamic inputs. With no fast inhibition, IE, the network responds easily to very few input spikes with little temporal correlation.

Note that the relative strengths of feedforward inhibition and excitation can shift the processing modality of the network. The connectivity within the local network can make a population of excitatory neurons sensitive to: 1) input timing alone, 2) input magnitude alone, 3) both, or 4) neither. The local network accomplishes these processing modalities by altering the convergence probabilities within local excitatory and inhibitory populations.

The hybrid network also bridges the gap in understanding the structure and function of the network. As observed in single neurons, where a broad range of covarying maximum channel conductances give rise to similar functional outputs (Prinz et al., 2004), a broad range of covarying network parameters can also give rise to the same functional effect of the network. Here, we focused on the convergence probabilities of feedforward inhibition and recurrent excitation, and found that multiple combinations of these parameters result in similar selectivity to input conditions (Kyriazi and Simons, 1993). In particular, damping networks are more sensitive to input timing and less sensitive to input magnitude, regardless of the specific synaptic convergence (Fig. 6C). Other parameters that could be

manipulated are total neuron number, ratio of excitatory and inhibitory neurons, and excitatory/inhibitory PSP amplitude. Although these manipulations may alter the fine-scale results, the general principles elucidated here will hold true.

The fast, reliable, and broadly tuned responses of FS neurons (Pesavento et al., 2010) are an essential component of transforming the temporal signature of thalamic input into a spike count (Pinto et al., 2003, 2000). Confirming earlier results, FS neurons respond earlier than RS neurons (Pesavento et al., 2010), giving rise to strong inhibition occurring 5-10 ms after initiation of thalamic input (Fig 1G). This requires more excitatory thalamic inputs to be able to generate a response within this narrow window of opportunity. Fast thalamic inputs have more spikes within the early portion of the response, so are able to withstand the rapid and strong inhibition from FS neurons. Conversely, slow inputs are more temporally distributed, and although feedforward inhibition will still lag behind the majority of excitatory thalamic synapses, it requires a proportionally much greater number of input spikes to generate a response of the same probability as with the fast inputs (Fig 2B). Thus, strong temporal correlation of thalamic input will result in a higher probability of response from the excitatory neuronal population. The results shown here confirm and extend the results from previous studies (Wilent and Contreras, 2004; Arabzadeh et al., 2003) by explicitly showing the contributions of feedforward inhibition, recurrent excitation, and the timing of thalamic input in the shaping of cortical responses.

*Neuronal membrane properties modulate effect of network connectivity*

The layer 4 barrel network responds preferentially to fast correlated input from thalamus, exhibiting reduced sensitivity to input magnitude (Fig.3; Pinto et al, 2000). This is in contrast to observations of individual neurons acting outside the context of a connected network (Pesavento et al., 2010). Here, by altering the intrinsic membrane properties of neuronal subpopulations, we have been able

878 to elucidate a crucial role of neuronal properties in shaping the population responses of excitatory barrel
879 neurons to thalamic input.

880 Few studies have examined the reciprocal effect of how the membrane properties of participating
881 neurons affect the response properties of the network. Our results suggest that network connections serve
882 to modify response properties already inherent in individual neurons. The presence of network
883 connections serves to shape the input received by a single neuron; that neuron will then respond in a
884 manner dictated by its intrinsic membrane properties (Pesavento et al., 2010). By altering the mean leak
885 conductance of a neuronal subpopulation, we alter how it responds to excitatory and inhibitory synaptic
886 input. To capture this idea, we introduced the concept of network sensitivity gain, which elucidates how
887 the intrinsic properties of individual neurons shape the effect of the local network in processing transient
888 stimuli.

889 The difference of RS and FS intrinsic membrane properties within the barrel network is sufficient
890 to establish the network's preference for input timing versus input magnitude. When excitatory and
891 inhibitory neurons have identical membrane properties (RS-RSi network), network connections have little
892 effect on network function. Such networks exhibit sensitivity to input timing and magnitude similar to
893 those in neurons without network connections (Fig 8B, C).

894 A key difference between RS and FS neuron intrinsic membrane properties is input resistance
895 (Pesavento et al., 2010). The hybrid network allowed us to manipulate the leak conductance in simulated
896 neurons, thus directly altering the membrane input resistance and time constant of all neurons within a
897 subpopulation. Simulated FS neurons with high leak conductance were associated with a decrease of
898 sensitivity to input timing of *in vitro* RS neurons embedded in the hybrid network. Interestingly,
899 increasing the difference of leak conductance between RS and FS values (via low gleakE and high gleakI)
900 resulted in RS neuron sensitivities to input timing below values observed without network input (Fig. 9E).
901 Confirming this result, simulations showed that the input resistance of inhibitory neurons, as controlled

902 by leak conductance, modulates network sensitivity to input timing within the excitatory neuronal
903 population (Fig. 10C). Thus, changing the relative leak conductances between the excitatory and
904 inhibitory populations bestows the ability to substantially shift sensitivity to input timing. In combination
905 with the role of excitatory leak conductance in shaping sensitivity to input magnitude (Fig. 10F), it is
906 apparent that input resistance within a given neuronal subpopulation plays a direct part in modulating the
907 role of the network's response to transient input.

908 The leak conductance of the inhibitory FS neuronal subpopulation plays a significant role in
909 shaping the network responses; however, the dynamics underlying this mechanism are subtle. To clarify
910 these interactions, we examined the effect of leak conductance on single cell response properties. We
911 originally expected that lower leak conductance (higher input resistance, longer membrane time constant)
912 would result in an increase of inhibitory spike latency, yielding responses similar to those observed with
913 the inhibitory RS (RSi) neurons. However, we did not observe a significant change of inhibitory latency
914 (Fig. 11E). Unexpectedly, networks with high inhibitory leak conductance (low input resistance) in the
915 presence of network connections exhibited increased spike time variability (Fig 11F). This is in contrast
916 to observations where high leak conductance in the absence of network connections resulted in a decrease
917 of spike variability (Fig. 11G).

918 Inhibitory FS neurons typically respond rapidly, reliably, and with little preference to the timing
919 of thalamic inputs (Pesavento et al., 2010), resulting in narrow spike timing distributions (cf. Fig 7A),
920 which are then propagated to excitatory RS neurons via feedforward inhibition. It is clear that networks
921 containing inhibitory neurons with high leak conductance have reduced threshold sensitivity to timing,
922 which in turn results in reduced network sensitivity to input timing. This stems from the increased spike
923 time variability in high leak conductance FS neurons, and the corresponding equalization of input
924 threshold across different input times. With higher temporal variability of synaptic feedforward inhibition,
925 fewer active thalamic synapses are required to generate an action potential. This reduces the difference of
926 RS neuron input thresholds between fast, medium, and slow inputs (Fig. 11A), effectively decreasing the

927 threshold sensitivity to input timing within single neurons (Pesavento et al., 2010). This, in turn, tends to
928 equalize population spike probability across input timing distributions (c.f. Fig. 9D) and decreases the
929 role of the network in facilitating temporal selectivity. Thus, increased variability of inhibitory neurons
930 resulting from increased leak conductance will reduce the network selectivity to high temporal correlation
931 present in thalamic inputs (Fig 10C).

932 In our simulated RS and FS cortical neurons, the leak conductance parameter directly alters the
933 input resistance and membrane time constant. A multitude of mechanisms can persistently change the
934 input resistance in specific neuronal subpopulations. Balanced excitatory and inhibitory synaptic input
935 increases membrane permeability (Paré et al., 1998; Destexhe and Paré, 1999) and can alter the efficacy
936 of excitatory inputs (Mainen and Sejnowski, 1995; Prescott and De Koninck, 2003).Anesthesia can affect
937 neuronal excitability and input resistance through a multitude of mechanisms (MacIver and Roth, 1987;
938 Kendig et al., 1991; Ishizawa, 2007). Typically, general anesthetics reduce excitability by opening $K^+$
939 channels (Ishizawa, 2007), thus reducing membrane input resistance. The norepinephrine system, via the
940 locus coeruleus, can modulate neuronal excitability by modifying the input resistance of neuronal
941 subpopulations and thus the transformation of information within a local network (Bergles et al., 1996;
942 Constantinople and Bruno, 2011). Many other potential mechanisms may directly alter a neuron's
943 membrane resistance, including persistent sodium channels, ion channel trafficking, and the effects of
944 other neuromodulators, including acetylcholine, dopamine, and serotonin.

945 It must be noted that we have not exhaustively examined differences between RS and FS neurons.
946 In this study, we focused on how differences in the leak conductance between RS and FS neurons is
947 important, but RS and FS neurons have many other differences that are likely to also be important. For
948 example, RS and FS neurons have different radii for the soma, spike properties, and firing rate adaptation.
949 Although we are presenting our synaptic conductances as they are observed at the soma, RS and FS
950 neurons are likely to integrate synaptic input differently within their dendritic arbors.

951

952 *Utility and restrictions of the hybrid network*

953 The use of a hybrid network allows a unique comparison of biological neuronal responses to
954 predictions from simulations. However, there are several notable differences between our simulated
955 barrel-like network and an *in vivo* network. For instance, the spatial distribution of synapses along the
956 dendritic processes can explain some of the differences in our results compared to those *in vivo*. Rather
957 than depolarizing the soma all at once, as in current clamp stimulation within whole-cell recordings,
958 dendritic processing would result in thalamic input arriving at the soma in a form that is more spatially
959 diffuse, allowing time for a multiple spike response within the soma (Williams and Stuart, 2003). Due to
960 the nature of the transient input from thalamus, our network does not include: low-threshold spiking
961 (LTS) neurons which largely do not receive direct thalamic input (Gibson et al., Beierlein et al., 2003),
962 short term synaptic depression or facilitation (Chance et al., 1998; Sun et al., 2006; Beierlein et al., 2003;
963 Cruikshank et al., 2007), NMDA receptor dynamics (Hull et al., 2009), or gap junction coupling between
964 inhibitory interneurons (Mancilla et al., 2007; Gibson et al., 1999). Most of these component responses
965 occur over longer time scales than we are examining here. The presence of gap junctions would serve to
966 facilitate synchrony within the FS population, but would do so in response to ongoing activity and would
967 have minimal contribution to shaping the timing of feedforward inhibition for the responses we observe.

968 Background synaptic activity is not present in the simulated network; that is, we do not induce
969 spontaneous action potentials and thus activation of synaptic conductances. This is largely not present
970 within the *in vitro* neurons, as previously discussed in Methods. The network used would most closely
971 approximate that observed with an anesthetized animal. In such a preparation, there is a very low level of
972 background activity within the barrel circuit (Brecht and Sakmann, 2002). The presence of balanced
973 background excitatory and inhibitory conductances serves to reduce the input resistance of each neuron
974 (Destexhe et al., 1999, 2001), which will have similar effects to what we have shown in this study.

975 Other caveats with the use of dynamic clamp to present simulated synaptic input have been
976 discussed elsewhere (Pesavento et al., 2010). For example, we are not simulating short-term synaptic
977 depression or facilitation, and the current applied on the soma may act differently than synaptic current
978 distributed across the dendritic arbor. Despite these caveats, we feel that our method for simulating
979 thalamic and cortical network input provides a realistic probe for comparing the responses of neurons
980 when acting alone versus when they are functioning as part of the barrel circuit.

981 Although it may not be surprising that neuronal population responses depend on both neuronal
982 and network properties, few studies have examined the reciprocal regulation of response selectivity as we
983 have done. Many studies focus either on single neuron response properties or on network level
984 interactions. Our results, however, suggest that neither approach is sufficient to fully understand circuit
985 function. Network connections serve to modify response properties already apparent in individual
986 neurons. Moreover, networks are more plastic than individual neurons, enabling the system to adapt its
987 responses to different conditions. On the other hand, the effect of the network also depends on the
988 membrane properties of participating neurons; when all of the neurons are the same, the network effects
989 are significantly reduced. Moreover, when the properties of one subclass are altered within the network –
990 as with leak conductance in FS neurons – such a change can modulate the timing and coherence of
991 inhibition, thus altering the effect of the local network. The properties of neuronal subpopulations thus
992 modulate the role of local network synapses, which in turn shape the output of the individual neurons.

993 Ultimately, the effect of the network comes down to how it shapes the input to individual neurons
994 via the timing and strength of excitatory and inhibitory synapses. Neurons, in turn, respond to the total
995 input both from thalamus and the local network in a manner consistent with their own properties. The
996 novel approach used here allows us to explain how the effect of feedforward inhibition depends on the
997 properties of single neurons, namely that RS neuron response latencies are more sensitive to the timing of
998 input compared to the responses of inhibitory FS neurons (Pesavento et al., 2010). The intrinsic
999 membrane properties of neuronal subpopulations are doing two things: shaping the input they receive

from the network via local synaptic convergence properties, and determining how the cell responds to that input via membrane properties. Although the underlying mechanisms are reciprocally intertwined, this constitutes a simple mechanism by which a neuron filters and responds to input, providing multiple degrees of fine control over the processing abilities of cortical networks.

## FIGURE LEGENDS

**Figure 1: Hybrid networks and simulating whisker-evoked volleys of thalamic input *in vitro*.**

**(A)** Conductance-based computational models of excitatory (E) and inhibitory (I) barrel neurons receive simulated synaptic conductances from thalamic inputs. Synaptic conductances are summed and passed to an *in vitro* (R) neuron via a conductance clamp. The in vitro neuron receives synaptic conductances from either thalamic inputs alone (left panel), or thalamic inputs as well as synaptic conductances from the simulated barrel neurons (center panel). Synaptic conductances are also applied from the real neuron back to the simulated network. The hybrid network allows easy alteration of membrane parameters across a neuronal subclass, such as giving all inhibitory cells the same membrane properties as RS neurons (right panel **(B)** Population spike time histograms from *in vivo* neurons (n=63) in response to caudal whisker deflections at three different velocities (fast, 2300°/s; medium, 1666°/s; slow, 800°/s), with 630 responses per histogram (adapted from Pinto et al., 2000). **(C)** Probability density functions (PDF) used to generate thalamic input spike times, quantified by the median time of the skewed distribution. Spike density histograms with 600 spikes per distribution are shown in panel **(D)**, and show similar characteristics to in vivo thalamic responses. **(E)** An example of the evoked excitatory post-synaptic potential of an RS neuron *in vitro* in response to a single simulated synaptic input. **(F)** Average synaptic conductance envelopes presented to an *in vitro* neuron with 15 thalamic input spikes (at threshold T) from 25 repetitions of fast, medium, and slow thalamic input distributions. **(G)** Average total ($G_{syn}$, black) and component synaptic conductance envelopes presented to an *in vitro* neuron with 26 thalamic input spikes (at threshold T). Strong inhibition ($g_I$ , red) follows the thalamic inputs ($g_{thal}$, blue), with weak recurrent excitation ($g_E$, green) occurring just after the inhibition. **(H)** The estimated synaptic reversal potentials ($\hat{E}_{syn}$) for thalamic input alone (left) and thalamic + network input (right). With thalamic input alone, only excitatory synapses are activated, giving rise to a constant reversal potential ($E_{AMPA}$). In the presence of network connections, the timing of inhibitory input sharply hyperpolarizes the reversal potential, decreasing the driving force.

**Figure 2: Effect of network connectivity on single neuron response measures.**

**(A)** Voltage traces of an example *in vitro* RS neuron over fast, medium, and slow simulated thalamic inputs at threshold T in the absence (thalamic input) or presence (thalamic+network) of hybrid network connections. The presence of strong feedforward inhibition is apparent in the hyperpolarization in the presence of network connections. **(B)** The probability of action potential generation for each thalamic input magnitude (the abscissa), input timing (fast, blue; medium, red; slow, green), and absence (dashed, hollow) or presence (solid, filled) of local hybrid network connections, averaged over 25 trials. Input threshold (T) for thalamic input alone (gray arrow) and thalamic+network input (filled arrow) are shown at the magnitudes yielding spike probabilities closest to 0.5 for the medium timing. The presence of network connections serves to increase the input threshold T, increases the dynamic range of input magnitudes, and separates the probability of action potential generation over thalamic input timing. **(C)** Mean response latency across input timing in the absence (gray) or presence (black) of hybrid network connections. Input magnitude is at threshold T. **(D)** Mean response variability across input timing, as in (C). The presence of network connections decreases response latency and variability for this example RS neuron.

**Figure 3: Effect of hybrid network connections on *in vitro* excitatory population responses.**

**(A-C)** Population spike density plots of 39 *in vitro* RS neurons with thalamic inputs (A), thalamic and network inputs (B), and *in vivo* (C), in response to thalamic inputs varied over timing (Fast, Medium, and Slow) and magnitude; simulated thalamic inputs are centered around input threshold T, while *in vivo* magnitudes are defined by the whisker displacement angle (Pinto et al., 2000). Spike counts are normalized by the number of spikes per stimulus that occur within a 100 μs bin. **(D-F)** The mean population responses of excitatory RS neurons for the same network conditions as in A-C. Lines connect

responses to stimulus presentations of a given magnitude (T-3, green; T/2.6°, blue; T+3/4.5°, red; T+6/7.4°, black) over the input timing, quantified as the time to the median of the thalamic input distribution (2 ms, fast; 5 ms, medium; 8 ms slow). Data in panels C and F are based on Pinto et al 2000. **(G)** Sensitivity to input timing, defined as the timing slope of the linear plane fit over the data shown in panels D-F. Sensitivity to input timing is significantly higher in the presence of local hybrid network input (t-test, $p<0.001$), while the *in vivo* sensitivity is similar to the responses we observe with the hybrid network. **(H)** Sensitivity to input magnitude, defined as the magnitude slope of the linear plane fit over the data in D-F. Sensitivity to input magnitude is significantly lower local hybrid network input (t-test, $p<0.001$). **(I)** The average population input threshold in the absence and presence of local network input; the threshold is significantly higher with the hybrid network (t-test, $p<0.001$). Error bars are ±SEM.

**Figure 4: Effect of connectivity on hybrid network neuron population response.**

Population responses in spikes per stimulus of excitatory RS neurons (n=10) for thalamic input alone, normal (IE=0.7, o) and low (IE=0.3, -) feedforward inhibition, and normal (EE=0.15, o) and high (EE=0.5, +) recurrent excitation (EE) convergence probabilities. **(A, B)** RS population responses in the hybrid network with network connections off and on (black and open, respectively, in panels F-G). **(C)** Population responses with weak IE and normal EE (solid gray in panels F-G); note the broadening of responses between different input magnitudes. **(D)** Population responses with normal IE and strong EE (striped white in panels F-G). **(E)** Population responses with weak IE and strong EE (striped gray in panels F-G); note the flatter lines across timing and broadening of responses between magnitudes. **(F)** Comparison of population sensitivity to input timing over the five hybrid network conditions. Population sensitivity to input timing with weak IE (gray) is significantly lower than with normal connectivity (white) (t-test, $p<0.001$ for both). Increasing EE does not have a significant effect. **(G)** Comparison of population sensitivity to input magnitude. Population sensitivity to input magnitude with weak IE and

strong EE (striped green) is significantly higher than normal connectivity (red) (t-test, $p<0.001$). Error bars are ±SEM.

**Figure 5: Simulated barrel network response sensitivity to changes in synaptic convergence.**

Population responses of 35 simulated RS neurons in response to simulated thalamic input alone **(A)** and connected in the local network **(B)**. Population responses are comparable to those observed in real RS neurons (cf. Fig 3D-E). Panels C-F show response sensitivity in both simulated (black) and hybrid (red) excitatory populations over different feedforward inhibition (IE) and recurrent excitation (EE) convergence probabilities. EE is fixed at 0.15 for C and E as IE changes; IE is fixed at 0.7 for D and F as EE changes. **(C)** Sensitivity to input timing increases as IE convergence increases over a broad range, matching the change of sensitivity observed in the hybrid networks. **(D)** Increasing EE convergence had no effect on either simulated or hybrid network response sensitivity to input timing. **(E)** Increasing IE convergence results in decreasing sensitivity to input magnitude, closely matching response sensitivity from the hybrid network. **(F)** Increasing EE convergence increases sensitivity to magnitude weakly over low values, and strongly for values greater than 0.5. **(G)** Surface plot of the sensitivity to input timing for different values of feedforward inhibition (IE) and recurrent excitation (EE) convergence values. Response sensitivity to input timing primarily depends on feedforward inhibition, so long as recurrent excitation is not too strong. **(H)** Surface plot of the sensitivity to input magnitude over different values of IE and EE. As IE decreases and EE increases, sensitivity to input magnitude increases dramatically. Further analysis of strong EE networks suggest that these are not damping networks (Pinto et al., 2003), and lead to multiple spikes and epileptiform activity. Error bars are ±SEM.

**Figure 6: Effect of network gain on response sensitivity of simulated networks.**

The upper panels show the response sensitivity to input timing **(A)** and input magnitude **(B)** for a *damping* network (network gain ratio=0.43, IE=0.9, EE=0.1), and an *amplifying* network (network gain ratio=1.17; IE=0.1, EE=0.35). In the presence of network connections (ON), the damping network exhibits significantly higher sensitivity to input timing (t-test, $p<0.001$), while there is no change in the amplifying network. The damping network is significantly less sensitive to input magnitude in the presence of network connections (t-test, $p<0.001$), while the amplifying network is significantly more sensitive (t-test, $p<0.001$). Error bars are ±SEM. **(C)** Scatter plot of the normalized sensitivity to input timing (blue) and input magnitude (red), as a function of the network gain for all network configurations examined. The sensitivity measures are normalized to the sensitivity with the network OFF; a value of 1 indicates no change, greater than one indicates an increase of sensitivity in the presence of network connections, less than one indicates a decrease of sensitivity. The arrows and black dots indicate the sensitivity based on the default "barrel-like" IE and EE connectivity values used (IE=0.7, EE=0.15).

**Figure 7: Difference of simulated population activity with FS or RSi neurons.**

**(A)** Spike raster plots and spike density graphs for simulated networks containing RS and FS neurons in the presence (thalamic + RS-FS) or absence (thalamic input alone) of simulated network connections. The spike raster plots show the responses of 35 simulated RS neurons and 15 simulated FS neurons in response to fast thalamic inputs at threshold T, with spike times indicated by the dashes. The number of thalamic input spikes required to reach threshold is shown (T). The spike density graphs are aligned in time with the raster plots, and show the combined response of 35 simulated RS neurons (black) and 15 simulated FS neurons (red), pooled over 25 stimulus presentations of fast simulated thalamic inputs. Spike counts are normalized by number of spikes per stimulus within a 100 μs bin. **(B)** Average total ($G_{syn}$, black) and component synaptic conductance envelopes exemplify typical synaptic inputs presented to a simulated or RS neuron *in vitro*. Thalamic conductance generated from 26 thalamic input spikes at threshold T ($g_{thal}$, blue), is closely followed by strong inhibition ($g_I$, red) and recurrent excitation ($g_E$,

green). Conductance envelopes are shown for fast, medium, and slow thalamic input distributions, with identical number of thalamic inputs. **(C)** Similar to B, showing the average synaptic conductance envelopes presented to an FS neuron. **(D)** The estimated synaptic reversal potentials ($E_{syn}$) for fast, medium, and slow thalamic inputs. The timing of recurrent excitation slows the hyperpolarization of the reversal potential, particularly for fast inputs (arrow). **(E)** Similar to D. Note the sustained depolarization and increased difference of hyperpolarization return time across thalamic input timing. **(F)** Similar to A, except that the FS neurons have been replaced by RS neurons while retaining the same inhibitory synapses and network parameters as the FS neurons. Note that with thalamic input alone, the RSi neurons (red) display the same spike density profile as the RS neurons (black), as expected. In the presence of network input (thalamic + RS-RSi), the spike density profiles overlap, with increased late responses in the RSi neurons. **(G)** Similar to B. Note the late occurrence of $g_I$ (red) relative to both thalamic (blue) and recurrent excitation (green) conductances. **(H)** Similar to D. The estimated synaptic reversal potential remains depolarized for longer than in C, and rapidly hyperpolarizes to the GABA reversal potential.

**Figure 8: Effect of intrinsic membrane properties of inhibitory neurons on hybrid network excitatory population responses.**

Excitatory population responses from 10 *in vitro* RS neurons embedded in either RS-FS hybrid networks (**A** and **B**) or RS-RSi hybrid networks (**C** and **D**) either in the absence (A and C) or presence (B and D) of simulated network connections. Lines connect responses to stimulus presentations of a given magnitude (T-3, green; T, blue; T+3, red; T+6, black) over the input timing, quantified as the time to the median of the thalamic input distribution (2 ms, fast; 5 ms, medium; 8 ms, slow). The top row is comparable to Figure 4A,B. **(E)** Sensitivity to input timing, measured as the slope over timing of the plane fit to the population response data shown in A. Networks with FS neurons show significantly higher sensitivity to input timing in the presence of network connections ($p<0.001$, t-test), while RSi networks do not show a significant change. **(F)** Sensitivity to input magnitude, calculated as the slope over magnitude of the plane

fit to the population response data in A. FS networks exhibit a significant decrease of sensitivity to input magnitude ($p<0.001$, t-test), while RSi networks exhibit a reduction of the sensitivity to input magnitude ($p=0.013$, t-test). Error bars are ±SEM.

**Figure 9: Effect of leak conductance on hybrid network population responses.**

Averaged excitatory population responses from 11 *in vitro* RS neurons embedded in hybrid networks in the absence **(A)** or presence of network connectivity (B-D). Leak conductance values are as follows (in $mS/cm^2$): gleakE, normal=0.057, low= 0.025, high=0.11; gleakI, normal=0.25, low=0.1, high=0.4. **(B)** Under barrel-like leak conductance (gleak) for both excitatory and inhibitory populations, the network exhibits sensitivity to input timing (slope of lines) and reduced sensitivity to input magnitude (spacing of lines). **(C)** Excitatory leak conductance (gleakE) is reduced in all simulated RS neurons, resulting in little apparent change of population response. **(D)** In combination with the low gleakE, inhibitory leak conductance (gleakI) is increased, resulting in relative insensitivity to input timing. We quantify the population sensitivity to input timing **(E)** and input magnitude **(F)** for the same 11 *in vitro* RS neurons across all conductance conditions. A circle (o) indicates normal barrel-like leak conductances, minus (-) indicates low gleak, plus (+) indicates high gleak. Bar shading matches the direction of excitatory leak conductance (gleakE). Error bars are ±SEM.

**Figure 10: Effect of leak conductance on simulated network response sensitivity**

Sensitivity to input timing of 35 simulated RS neurons over changes of inhibitory leak conductance (gleakI) **(A)** or changes of excitatory leak conductance (gleakE) **(B)**, in the absence (dashed, hollow) or presence (solid, filled) of network connections. Note that in (B), changes of gleakE have a direct effect on sensitivity to input timing in both the presence or absence of network connections. To isolate the effect of the network, we normalize the measure to that with the network off, giving us the *network sensitivity gain*

for input timing (C-D) and input magnitude (E-F). Linear regression lines are drawn through each plot, and the significance of the regression slope is given (p-value of ANOVA). Increasing gleakI significantly decreases the network's effect on sensitivity to input **(C)** while having no effect on the sensitivity to input magnitude **(E)**. Increasing gleakE slightly decreases the network sensitivity to input timing **(D)**, and strongly decreases the sensitivity to input magnitude **(F)**. Error bars are ±SEM.

**Figure 11: Changes in gleakI alter single neuron response measures in simulation**

Single neuron input threshold, spike latency, and spike variability of simulated RS and FS neurons were measured across fast (black), medium (red), and slow (blue) input timing distributions for increasing values of leak conductance of inhibitory neurons (gleak I). Simulated RS neurons in the presence of network connectivity (net on) showed **(A)** a decrease of input threshold to slow inputs and a slight increase to fast inputs, with little change of latency **(B)** or variability **(C)**. With increasing gleakI, simulated FS neurons showed **(D)** an increase of input threshold for both network off (net off; dashed lines, hollow shapes) and network on (net on; solid lines and shapes). **(E)** In the absence of network connections, spike latency slightly decreased with increasing gleakI, while in the presence of network connections slightly increased for slow thalamic inputs. **(F)** The presence of local network synapses increases spike variability, especially for slow thalamic inputs. **(G)** The absence of network synapses decreases spike variability, as expected from the increase in input threshold. Error bars are ±SEM.

**Table 1: Comparison of real and simulated single neuron response measures**

Single neuron response threshold, latency, and variability in real RS neurons (N=39) and simulated RS neurons (N=35) as a function of network connectivity (OFF versus ON). Values are mean ±SEM. An asterisk (*) indicates statistical significance ($p<0.01$, pairwise t-test) between network OFF and ON.

| | | in vitro | | sim | |
|---|---|---|---|---|---|
| | | net OFF | net ON | net OFF | net ON |
| mean | threshold (# spikes) | 16.7 ± 0.8 | 29.0 ± 1.7 | 14.6 ± 0.04 | 24.9 ± 0.06 |
| | latency (ms) | 9.8 ± 0.4 | 6.8 ± 0.15 | 13.3 ± 0.1 | 9.6 ± 0.04 |
| | variability (ms) | 1.95 ± 0.17 | 1.11 ± 0.08 | 3.21 ± 0.07 | 2.38 ± 0.05 |
| | | | | | |
| sens. input timing | threshold (# spikes) | 0.41 ± 0.02 | 3.11 ± 0.33 | 0.32 ± 0.02 | 0.86 ± 0.02 |
| | latency (ms) | 1.27 ± 0.10 | 1.00 ± 0.03 | 1.43 ± 0.03 | 1.23 ± 0.02 |
| | variability (ms) | 0.28 ± 0.04 | 0.19 ± 0.02 | 0.22 ± 0.02 | 0.24 ± 0.02 |
| | | | | | |
| sens. input magnitude | latency (ms) | 0.56 ± 0.15 | 0.02 ± 0.012 | 0.65 ± 0.03 | 0.09 ± 0.01 |
| | variability (ms) | 0.24 ± 0.11 | 0.03 ± 0.011 | 0.23 ± 0.03 | 0.03 ± 0.013 |

**REFERENCES**


Adorján, P., Levitt, J. B., Lund, J. S., & Obermayer, K. (1999). A model for the intracortical origin of orientation preference and tuning in macaque striate cortex. *Visual Neuroscience*, *16*(2), 303-318.

Alonso, J.-M., Usrey, W. M., & Reid, R. C. (1996). Precisely correlated firing in cells of the lateral geniculate nucleus. *Nature*, *383*(6603), 815-819.

Arabzadeh, E., Zorzin, E., & Diamond, M. E. (2005). Neuronal encoding of texture in the whisker sensory pathway. *PLoS Biology*, *3*(1), e17

Azouz, R., & Gray, C. M. (2000). Dynamic spike threshold reveals a mechanism for synaptic coincidence detection in cortical neurons in vivo. *Proceedings of the National Academy of Sciences of the United States of America*, *97*(14), 8110-8115.

Beierlein, M., Gibson, J. R., & Connors, B. W. (2003). Two dynamically distinct inhibitory networks in layer 4 of the neocortex. *Journal of Neurophysiology*, *90*(5), 2987-3000.

Bergles, D. E., Doze, V. A., Madison, D. V., & Smith, S. J. (1996). Excitatory actions of norepinephrine on multiple classes of hippocampal CA1 interneurons. *Journal of Neuroscience*, *16*(2), 572-585.

Brecht, M., & Sakmann, B. (2002). Dynamic representation of whisker deflection by synaptic potentials in spiny stellate and pyramidal cells in the barrels and septa of layer 4 rat somatosensory cortex. *Journal of Physiology*, *543*(1), 49-70.

Bruno, R. M., & Sakmann, B. (2006). Cortex is driven by weak but synchronously active thalamocortical synapses. *Science*, *312*(5780), 1622-1627.

Buracas, G. T., Zador, A. M., DeWeese, M. R., & Albright, T. D. (1998). Efficient discrimination of temporal patterns by motion-sensitive neurons in primate visual cortex. *Neuron*, *20*(5), 959-969.

Castro-Alamancos, M. A. (2002). Different temporal processing of sensory inputs in the rat thalamus during quiescent and information processing states in vivo. *Journal of Physiology*, *539*(2), 567-578.

Chance, F., Nelson, S., & Abbott, L. (1998). Synaptic depression and the temporal response characteristics of V1 cells. *Journal of Neuroscience*, *18*(12), 4785-4799.

Chow, A., Erisir, A., Farb, C., Nadal, M., Ozaita, A., Lau, D., Welker, E., et al. (1999). K+ channel expression distinguishes subpopulations of parvalbumin-and somatostatin-containing neocortical interneurons. *Journal of Neuroscience*, *19*(21), 9332-9345. Soc Neuroscience.

1237 Chung, S., & Ferster, D. (1998). Strength and Orientation Tuning of the Thalamic Input to
1238 Simple Cells Revealed by Electrically Evoked Cortical Suppression. *Neuron*, *20*(6), 1177-
1239 1189.

1240 Coetzee, W. A., Amarillo, Y., Chiu, J., Chow, A., Lau, D., McCORMACK, T., Morena, H., et al.
1241 (1999). Molecular diversity of K+ channels. *Annals of the New York Academy of Sciences*,
1242 *868*, 233–255.

1243 Constantinople, C. M., & Bruno, R. M. (2011). Effects and Mechanisms of Wakefulness on
1244 Local Cortical Networks. *Neuron*, *69*(6), 1061-1068.

1245 Cruikshank, S. J., Urabe, H., Nurmikko, A. V., & Connors, B. W. (2010). Pathway-specific
1246 feedforward circuits between thalamus and neocortex revealed by selective optical
1247 stimulation of axons. *Neuron*, *65*(2), 230-45.

1248 Cruikshank, S., Lewis, T., & Connors, B. (2007). Synaptic basis for intense thalamocortical
1249 activation of feedforward inhibitory cells in neocortex. *Nature Neuroscience*, *10*(4), 462-
1250 468.

1251 de Kock, C. P. J., Bruno, R. M., Spors, H., & Sakmann, B. (2007). Layer- and cell-type-specific
1252 suprathreshold stimulus representation in rat primary somatosensory cortex. *The Journal of*
1253 *physiology*, *581*(Pt 1), 139-54.

1254 DeWeese, M. R., Wehr, M., & Zador, A. M. (2003). Binary Spiking in Auditory Cortex. *J*
1255 *Neuroscience*, *23*(21), 7940-7949.

1256 Destexhe, A., Bal, T., McCormick, D. A., & Sejnowski, T. J. (1996). Ionic mechanisms
1257 underlying synchronized oscillations and propagating waves in a model of ferret thalamic
1258 slices. *J Neurophysiology*, *76*(3), 2049-2070.

1259 Destexhe, A., Mainen, Z. F., & Sejnowski, T. J. (1998). Kinetic models of synaptic transmission.
1260 In C. Koch & I. Segev (Eds.), *Methods in Neuronal Modeling* (2nd ed., pp. 1-26).
1261 Cambridge, Massachusetts: The MIT Press.

1262 Destexhe, A., & Pare, D. (1999). Impact of Network Activity on the Integrative Properties of
1263 Neocortical Pyramidal Neurons In Vivo. *Journal of Neurophysiology*, *81*(4), 1531-1547.

1264 Destexhe, A., Rudolph, M., Fellous, J.-M., & Sejnowski, T. J. (2001). Fluctuating synaptic
1265 conductances recreate in vivo-like activity in neocortical neurons. *Neuroscience*, *107*(1),
1266 13-24.

1267 Douglas, R. J., Koch, C., Mahowald, M., Martin, K. A., & Suarez, H. H. (1995). Recurrent
1268 excitation in neocortical circuits. *Science*, *269*(5226), 981-985. AAAS.

1269 Erisir, A., Lau, D., Rudy, B., & Leonard, C. S. (1999). Function of Specific K+ Channels in
1270 Sustained High-Frequency Firing of Fast-Spiking Neocortical Interneurons. *J Neurophysiol*,
1271 *82*(5), 2476-2489.

1272 Ermentrout, B. (1998a). Linearization of F-I Curves by Adaptation. *Neural Computation*, *10*(7),
1273 1721-1729.

1274 Ermentrout, B. (1998b). Neural networks as spatio-temporal pattern-forming systems. *Reports on*
1275 *Progress in Physics*, *61*(4), 353-430. doi:10.1088/0034-4885/61/4/002

1276 Fisk, P. R. (1961). The graduation of income distributions. *Econometrica*, *29*(2), 171-185.

1277 Gabernet, L., Jadhav, S. P., Feldman, D. E., Carandini, M., & Scanziani, M. (2005).
1278 Somatosensory integration controlled by dynamic thalamocortical feed-forward inhibition.
1279 *Neuron*, *48*(2), 315-327.

1280 Gibson, J. R., Beierlein, M., & Connors, B. W. (1999). Two networks of electrically coupled
1281 inhibitory neurons in neocortex. *Nature*, *402*(6757), 75-79.

1282 Goldberg, E. M., Clark, B. D., Zagha, E., Nahmani, M., Erisir, A., & Rudy, B. (2008). K+
1283 Channels at the Axon Initial Segment Dampen Near-Threshold Excitability of Neocortical
1284 Fast-Spiking GABAergic Interneurons. *Neuron*, *58*(3), 387-400.

1285 Golomb, D., & Amitai, Y. (1997). Propagating neuronal discharges in neocortical slices:
1286 computational and experimental study. *Journal of Neurophysiology*, *78*(3), 1199. Am
1287 Physiological Soc.

1288 Golomb, D., Donner, K., Shacham, L., Shlosberg, D., Amitai, Y., & Hansel, D. (2007).
1289 Mechanisms of firing patterns in fast-spiking cortical interneurons. *PLoS computational*
1290 *biology*, *3*(8), e156.

1291 Hausser, M., & Roth, A. (1997). Estimating the time course of the excitatory synaptic
1292 conductance in neocortical pyramidal cells using a novel voltage jump method. *Journal of*
1293 *Neuroscience*, *17*(20), 7606-7625.

1294 Hirsch, J. A., Alonso, J.-M., Reid, R. C., & Martinez, L. M. (1998). Synaptic integration in
1295 striate cortical simple cells. *Journal of Neuroscience*, *18*(22), 9517-9528.

1296 Hull, C., Isaacson, J. S., & Scanziani, M. (2009). Postsynaptic mechanisms govern the
1297 differential excitation of cortical neurons by thalamic inputs. *Journal of Neuroscience*,
1298 *29*(28), 9127-9136.

1299 Ishizawa, Y. (2007). Mechanisms of anesthetic actions and the brain. *Journal of Anesthesia*,
1300 *21*(2), 187-199.

1301 Ito, M., & Kato, M. (2002). Analysis of variance study of the rat cortical layer 4 barrel and layer
1302 5b neurones. *Journal of Physiology*, *539*(Pt 2), 511-522.

1303 Jensen, K., & Killackey, H. (1987). Terminal arbors of axons projecting to the somatosensory
1304 cortex of the adult rat. I. The normal morphology of specific thalamocortical afferents.
1305 *Journal of Neuroscience*, *7*(11), 3529-3543.

1306 Kawaguchi, Y. (1993). Physiological, morphological, and histochemical characterization of three
1307 classes of interneurons in rat neostriatum. *Journal of Neuroscience*, *13*(11), 4908-4923.

1308 Kawaguchi, Y., & Kubota, Y. (1997). GABAergic cell subtypes and their synaptic connections
1309 in rat frontal cortex. *Cerebral Cortex*, *7*(6), 476-486.

1310 Kendig, J. J., MacIver, M. B., & Roth, S. H. (1991). Anesthetic actions in the hippocampal
1311 formation. *Annals Of The New York Academy Of Sciences*, *625*, 37-53.

1312 Kleppe, I., & Robinson, H. (1999). Determining the activation time course of synaptic AMPA
1313 receptors from openings of colocalized NMDA receptors. *Biophysical Journal*, *77*(3), 1418-
1314 1427.

1315 Kopell, N., Ermentrout, G. B., Whittington, M. A., & Traub, R. D. (2000). Gamma rhythms and
1316 beta rhythms have different synchronization properties. *Proceedings of the National*
1317 *Academy of Sciences of the United States of America*, *97*(4), 1867-1872.

1318 Kyriazi, H. T., & Simons, D. J. (1993). Thalamocortical response transformations in simulated
1319 whisker barrels. *Journal of Neuroscience*, *13*(4), 1601-1615.

1320 Land, P., & Kandler, K. (2002). Somatotopic organization of rat thalamocortical slices. *Journal*
1321 *of Neuroscience Methods*, *119*(1), 15-21.

1322 Land, P. W., Buffer, S. A., & Yaskosky, J. D. (1995). Barreloids in adult rat thalamus: three-
1323 dimensional architecture and relationship to somatosensory cortical barrels. *Journal of*
1324 *Comparative Neurology*, *355*(4), 573-588.

1325 Lawrence, J., & McBain, C. (2003). Interneuron diversity series: containing the detonation-
1326 feedforward inhibition in the CA3 hippocampus. *Trends in Neurosciences*, *26*(11), 631-640.

1327 Lien, C. C., & Jonas, P. (2003). Kv3 potassium conductance is necessary and kinetically
1328 optimized for high-frequency action potential generation in hippocampal interneurons.
1329 *Journal of Neuroscience*, *23*(6), 2058-2068.

1330 Liu, B.-hua, Wu, G. K., Arbuckle, R., Tao, H. W., & Zhang, L. I. (2007). Defining cortical
1331 frequency tuning with recurrent excitatory circuitry. *Nature neuroscience*, *10*(12), 1594-
1332 600.

MacIver, M. B., & Roth, S. H. (1987). Anesthetics produce differential actions on membrane responses of the crayfish stretch receptor neuron. *European Journal of Pharmacology*, *141*(1), 67-77.

Mainen, Z. F., & Sejnowski, T. J. (1995). Reliability of spike timing in neocortical neurons. *Science*, *268*(5216), 1503-1506.

Mancilla, J. G., Lewis, T. J., Pinto, D. J., Rinzel, J., & Connors, B. W. (2007). Synchronization of electrically coupled pairs of inhibitory interneurons in neocortex. *Journal of Neuroscience*, *27*(8), 2058-2073.

McCormick, D. A., Connors, B. W., Lighthall, J. W., & Prince, D. A. (1985). Comparative electrophysiology of pyramidal and sparsely spiny stellate neurons of the neocortex. *Journal of Neurophysiology*, *54*(4), 782-806.

Miller, K. D., Pinto, D. J., & Simons, D. J. (2001). Processing in layer 4 of the neocortical circuit: new insights from visual and somatosensory cortex. *Current Opinion in Neurobiology*, *11*(4), 488-497.

Pare, D., Shink, E., Gaudreau, H., Destexhe, A., & Lang, E. J. (1998). Impact of Spontaneous Synaptic Activity on the Resting Properties of Cat Neocortical Pyramidal Neurons In Vivo. *Journal of Neurophysiology*, *79*(3), 1450-1460.

Pesavento, M. J., Rittenhouse, C. D., & Pinto, D. J. (2010). Response sensitivity of barrel neuron subpopulations to simulated thalamic input. *Journal of Neurophysiology*, *103*(6), 3001-3016. doi:10.1152/jn.01053.2009

Petersen, C. C. H., Grinvald, A., & Sakmann, B. (2003). Spatiotemporal dynamics of sensory responses in layer 2/3 of rat barrel cortex measured in vivo by voltage-sensitive dye imaging combined with whole-cell voltage recordings and neuron reconstructions. *Journal of Neuroscience*, *23*(4), 1298-1309.

Phillips, J., Johnson, K., & Hsiao, S. (1988). Spatial pattern representation and transformation in monkey somatosensory cortex. *Proceedings of the National Academy of Sciences*, *85*(4), 1317.

Pinto, D. J., Brumberg, J. C., & Simons, D. J. (2000). Circuit dynamics and coding strategies in rodent somatosensory cortex. *Journal of Neurophysiology*, *83*(3), 1158-1166.

Pinto, D. J., Hartings, J. A., Brumberg, J. C., & Simons, D. J. (2003). Cortical damping: analysis of thalamocortical response transformations in rodent barrel cortex. *Cerebral Cortex*, *13*(1), 33-44.

Pinto, D. J., Jones, S. R., Kaper, T. J., & Kopell, N. (2003). Analysis of state-dependent transitions in frequency and long-distance coordination in a model oscillatory cortical circuit. *Journal of Computational Neuroscience*, *15*(2), 283-298.

1368 Pouille, F., & Scanziani, M. (2001). Enforcement of temporal fidelity in pyramidal cells by
1369 somatic feed-forward inhibition. *Science*, *293*(5532), 1159-1163.

1370 Prescott, S. A., & De Koninck, Y. (2003). Gain control of firing rate by shunting inhibition: roles
1371 of synaptic noise and dendritic saturation. *Proceedings of the National Academy of Sciences*
1372 *of the United States of America*, *100*(4), 2076-81.

1373 Prescott, S. A., & Sejnowski, T. J. (2008). Spike-rate coding and spike-time coding are affected
1374 oppositely by different adaptation mechanisms. *Journal of Neuroscience*, *28*(50), 13649-
1375 13661.

1376 Prinz, A. A., Abbott, L., & Marder, E. (2004). The dynamic clamp comes of age. *Trends in*
1377 *Neurosciences*, *27*(4), 218–224.

1378 Reinagel, P., & Reid, R. C. (2000). Temporal Coding of Visual Information in the Thalamus. *J.*
1379 *Neuroscience*, *20*(14), 5392-5400.

1380 Sachdev, R. N. S., Ebner, F. F., & Wilson, C. J. (2004). Effect of subthreshold up and down
1381 states on the whisker-evoked response in somatosensory cortex. *Journal of*
1382 *Neurophysiology*, *92*(6), 3511-3521.

1383 Simons, D. J., & Carvell, G. E. (1989). Thalamocortical response transformation in the rat
1384 vibrissa/barrel system. *Journal of Neurophysiology*, *61*(2), 311-330.

1385 Skinner, F. K., Chung, J. Y. J., Ncube, I., Murray, P. A., & Campbell, S. A. (2005). Using
1386 heterogeneity to predict inhibitory network model characteristics. *Journal of*
1387 *Neurophysiology*, *93*(4), 1898-1907.

1388 Staiger, J. F., Flagmeyer, I., Schubert, D., Zilles, K., Kötter, R., & Luhmann, H. J. (2004).
1389 Functional diversity of layer IV spiny neurons in rat somatosensory cortex: quantitative
1390 morphology of electrophysiologically characterized and biocytin labeled cells. *Cerebral*
1391 *Cortex*, *14*(6), 690-701.

1392 Storm, J. F. (1988). Temporal integration by a slowly inactivating K+ current in hippocampal
1393 neurons. *Nature*, *336*(6197), 379-381.

1394 Sun, Q. Q., Huguenard, J. R., & Prince, D. A. (2006). Barrel cortex microcircuits:
1395 thalamocortical feedforward inhibition in spiny stellate cells is mediated by a small number
1396 of fast-spiking interneurons. *Journal of Neuroscience*, *26*(4), 1219-1230.

1397 Swadlow, H. A., Bezdudnaya, T., & Gusev, A. G. (2005). Spike timing and synaptic dynamics at
1398 the awake thalamocortical synapse. *Progress in Brain Research*, *149*, 91-105.

1399 Swadlow, H. A., & Gusev, A. G. (2002). Receptive-field construction in cortical inhibitory
1400 interneurons. *Nature Neuroscience*, *5*(5), 403-404.

1401 Toledo-Rodriguez, M., Blumenfeld, B., Wu, C., Luo, J., Attali, B., Goodman, P., & Markram, H.
1402 (2004). Correlation maps allow neuronal electrical properties to be predicted from single-
1403 cell gene expression profiles in rat neocortex. *Cerebral Cortex*, *14*(12), 1310-1327.

1404 Varga, C., Sík, A., Lavallée, P., & Deschênes, M. (2002). Dendroarchitecture of relay cells in
1405 thalamic barreloids: a substrate for cross-whisker modulation. *Journal of Neuroscience*,
1406 *22*(14), 6186-6194.

1407 Wehr, M., & Zador, A. M. (2003). Balanced inhibition underlies tuning and sharpens spike
1408 timing in auditory cortex. *Nature*, *426*(6965), 442-446.

1409 Welker, C. (1971). Microelectrode delineation of fine grain somatotopic organization of SmI
1410 cerebral neocortex in albino rat. *Brain Research*, *26*(2), 259-275.

1411 Welker, C., & Woolsey, T. A. (1974). Structure of layer IV in the somatosensory neocortex of
1412 the rat: Description and comparison with the mouse. *Journal of Comparative Neurology*,
1413 *158*(4), 437-453.

1414 Wilent, W. B., & Contreras, D. (2004). Synaptic responses to whisker deflections in rat barrel
1415 cortex as a function of cortical layer and stimulus intensity. *Journal of Neuroscience*,
1416 *24*(16), 3985-3998.

1417 Wilent, W. B., & Contreras, D. (2005). Stimulus-dependent changes in spike threshold enhance
1418 feature selectivity in rat barrel cortex neurons. *Journal of Neuroscience*, *25*(11), 2983-2991.

1419 Williams, S. R., & Stuart, G. J. (2003). Role of dendritic synapse location in the control of action
1420 potential output. *Trends in Neurosciences*, *26*(3), 147-154.

1421 Woolsey, T. A., & Van Der Loos, H. (1970). The structural organization of layer IV in the
1422 somatosensory region (S I) of mouse cerebral cortex: The description of a cortical field
1423 composed of discrete cytoarchitectonic units. *Brain Research*, *17*(2), 205-242.

1424

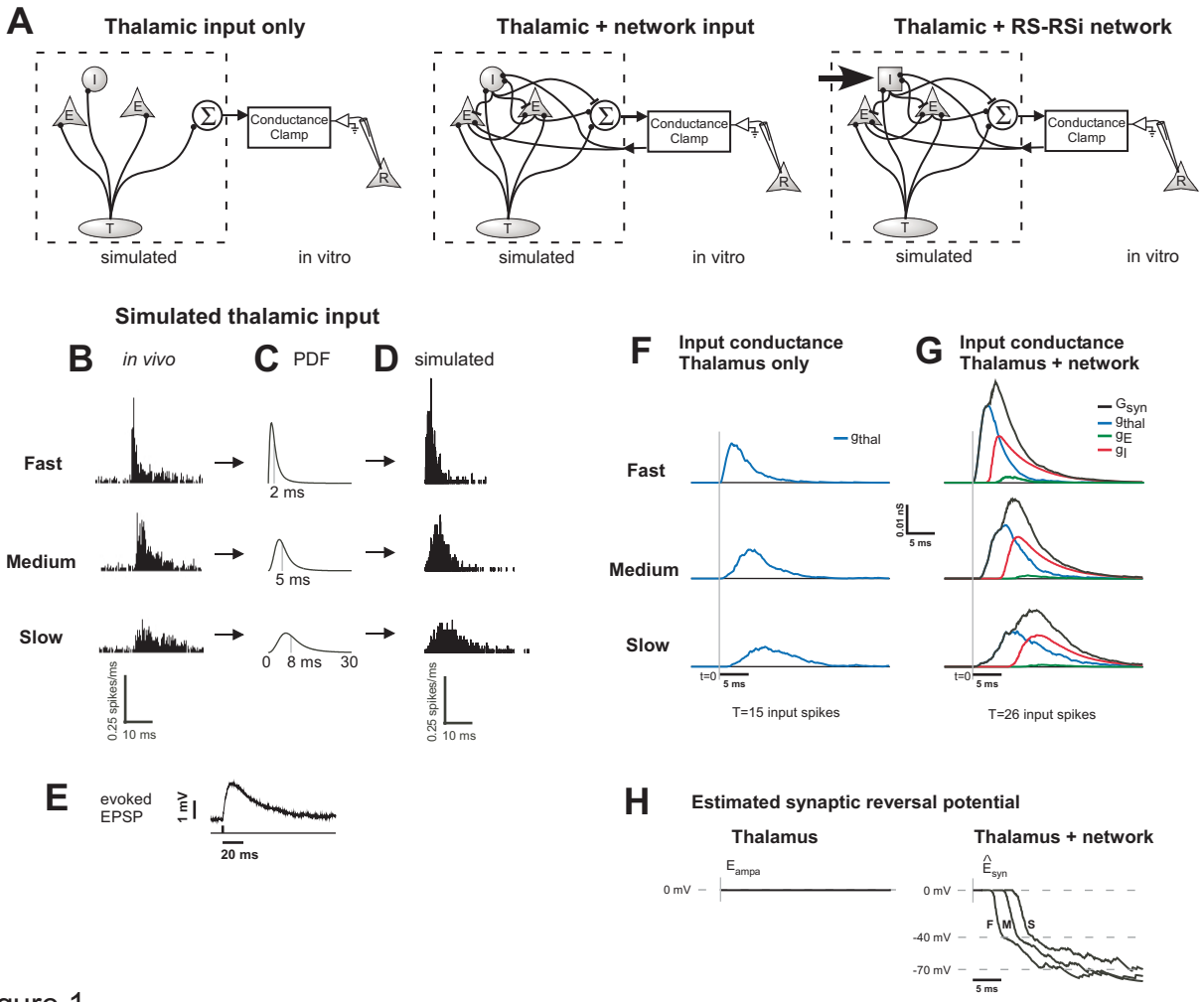
A
Thalamic input only
Thalamic + network input
Thalamic + RS-RSi network
Conductance Clamp
simulated
in vitro
Simulated thalamic input
B in vivo
C PDF
D simulated
Fast
Medium
Slow
2 ms
5 ms
0 8 ms 30
0.25 spikes/ms
10 ms
E
evoked EPSP
1 mV
20 ms
F Input conductance Thalamus only
G Input conductance Thalamus + network
gthal
Gsyn
gE
gI
0.01 nS
5 ms
t=0
T=15 input spikes
T=26 input spikes
H Estimated synaptic reversal potential
Thalamus
Thalamus + network
Eampa
Esyn
0 mV
-40 mV
-70 mV
F M S

figure 1

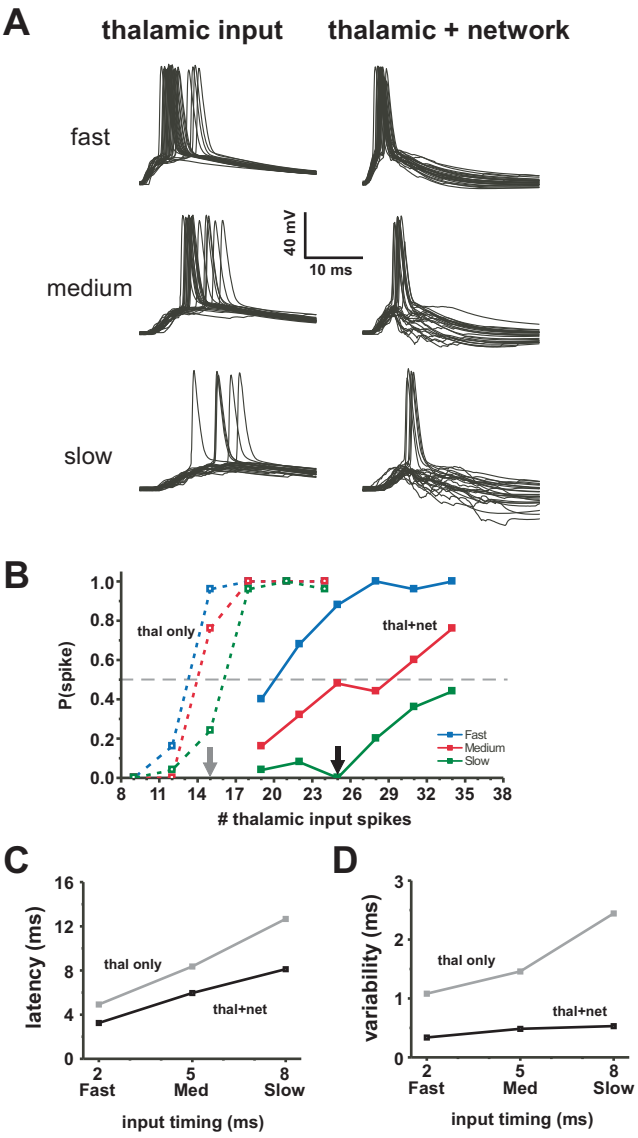
A
thalamic input
thalamic + network
fast
medium
slow
40 mV
10 ms
B
P(spike)
thal only
thal+net
Fast
Medium
Slow
# thalamic input spikes
C
latency (ms)
thal only
thal+net
Fast
Med
Slow
input timing (ms)
D
variability (ms)
thal only
thal+net
Fast
Med
Slow
input timing (ms)

figure 2

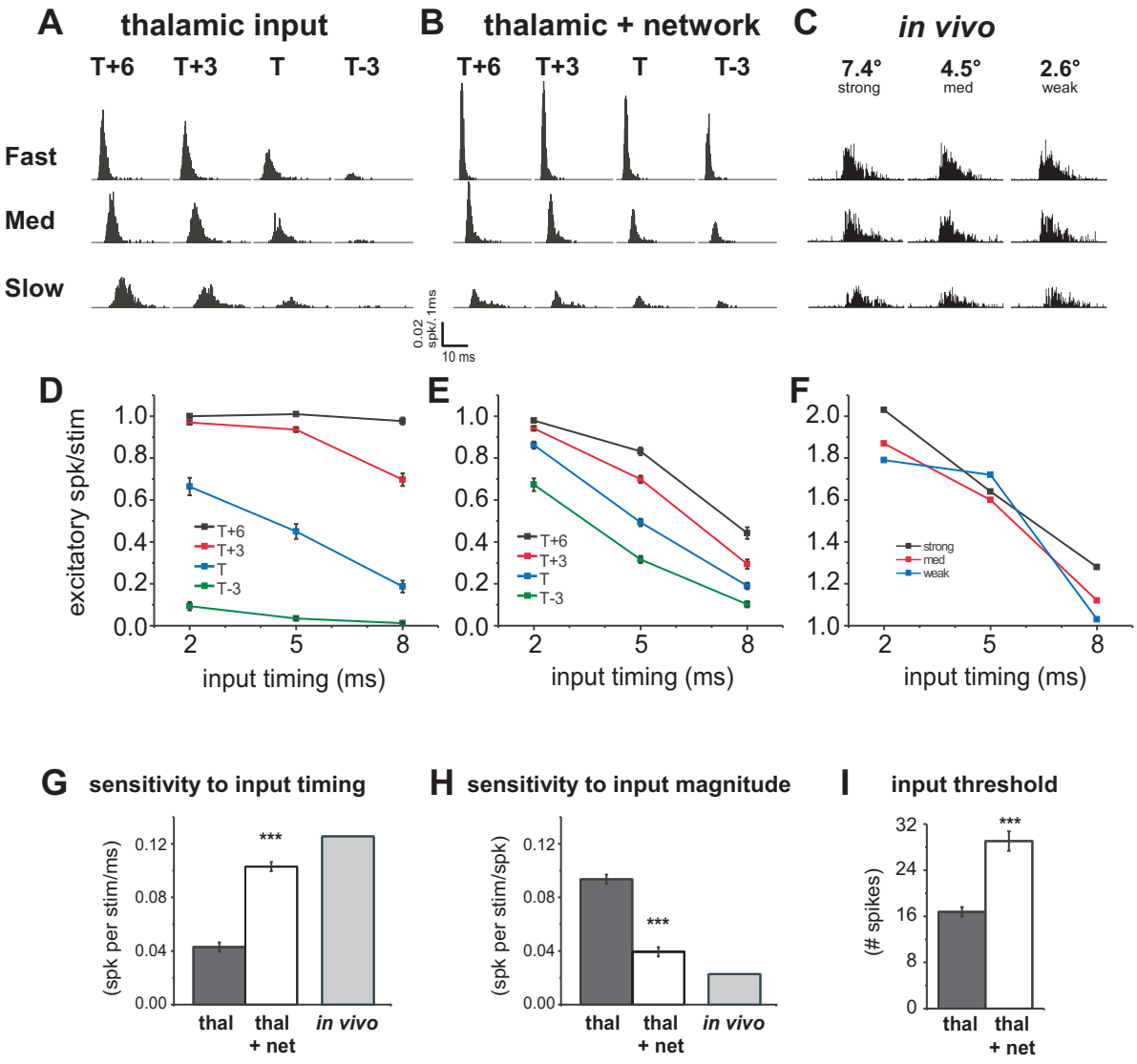
A
thalamic input
B
thalamic + network
C
in vivo
T+6
T+3
T
T-3
7.4°
strong
4.5°
med
2.6°
weak
Fast
Med
Slow
0.02 spk/.1ms
10 ms
D
E
F
excitatory spk/stim
input timing (ms)
T+6
T+3
T
T-3
strong
med
weak
G
sensitivity to input timing
H
sensitivity to input magnitude
I
input threshold
(spk per stim/ms)
(spk per stim/spk)
(# spikes)
***
thal
thal + net
in vivo

figure 3

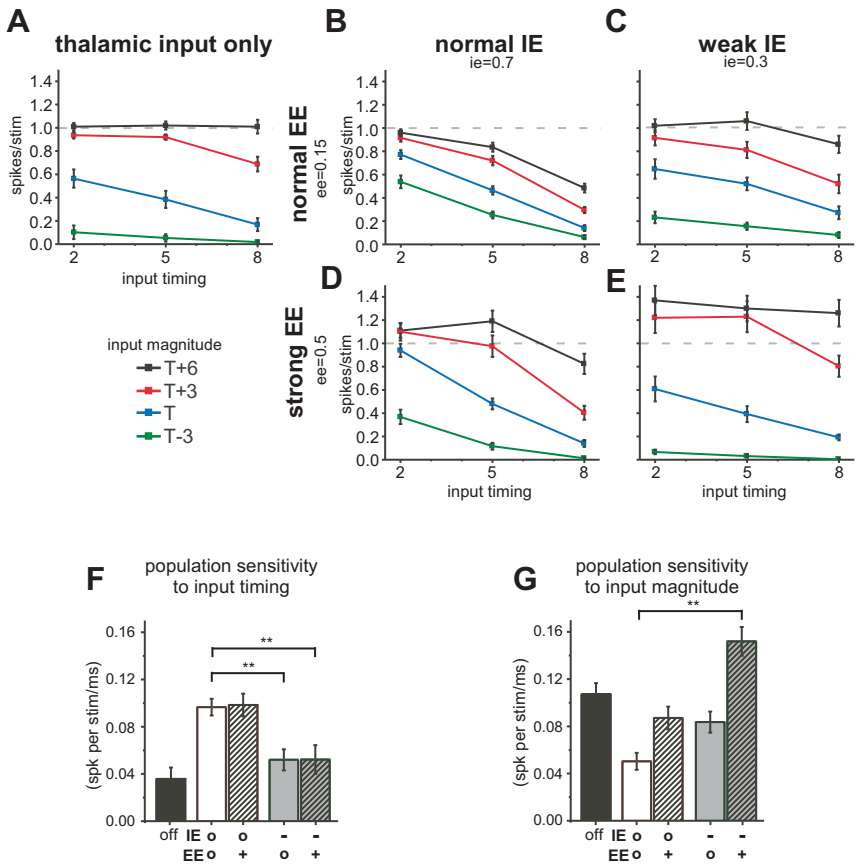
A
thalamic input only
B
normal IE
ie=0.7
C
weak IE
ie=0.3
normal EE
ee=0.15
strong EE
ee=0.5
D
E
spikes/stim
input timing
input magnitude
T+6
T+3
T
T-3


F
population sensitivity
to input timing
G
population sensitivity
to input magnitude
(spk per stim/ms)
off
IE
EE
**

figure 4

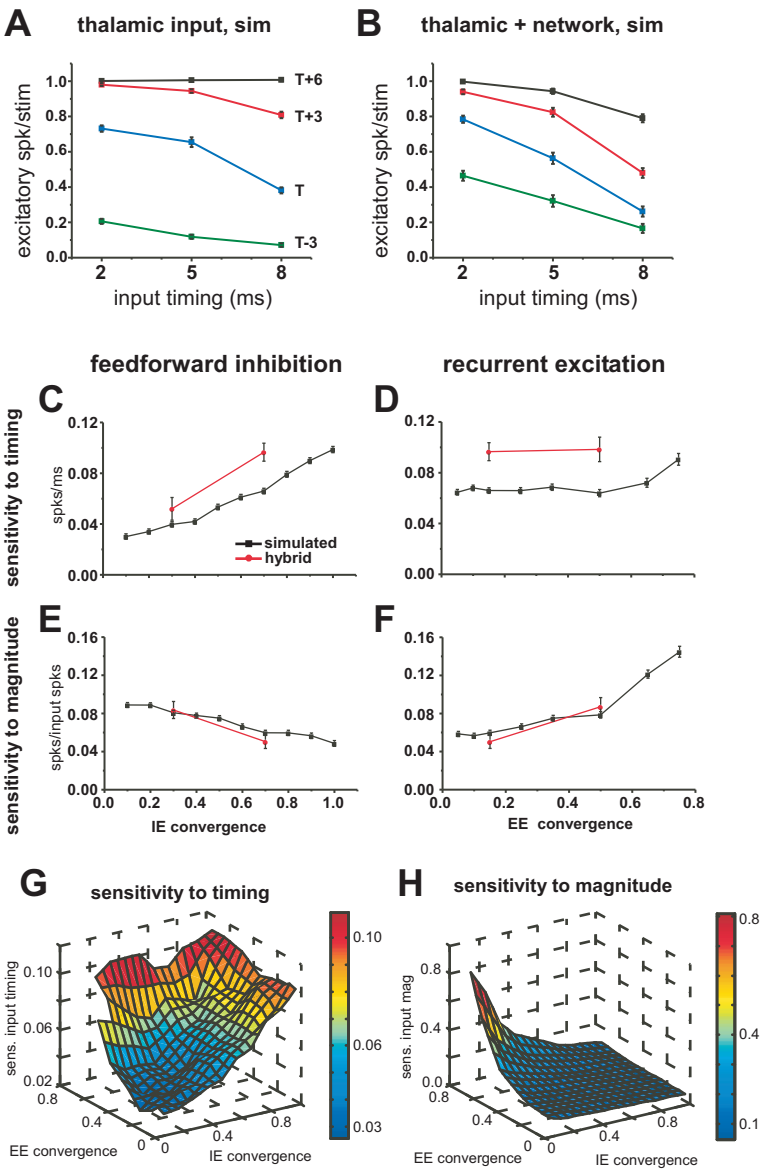
A
thalamic input, sim
B
thalamic + network, sim
excitatory spk/stim
input timing (ms)
T+6
T+3
T
T-3
feedforward inhibition
recurrent excitation
C
D
E
F
sensitivity to timing
sensitivity to magnitude
spks/ms
spks/input spks
simulated
hybrid
IE convergence
EE convergence
G
H
sensitivity to timing
sensitivity to magnitude
sens. input timing
sens. input mag
EE convergence
IE convergence

figure 5

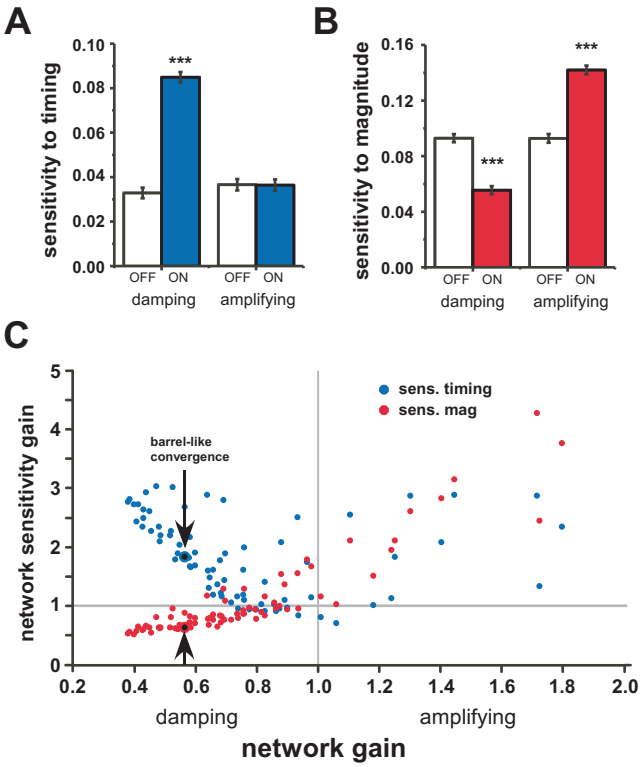
A
B
C
sensitivity to timing
0.10
0.08
0.06
0.04
0.02
0.00
***
OFF ON
damping
OFF ON
amplifying
sensitivity to magnitude
0.16
0.12
0.08
0.04
0.00
***
***
OFF ON
damping
OFF ON
amplifying
network sensitivity gain
5
4
3
2
1
0
sens. timing
sens. mag
barrel-like
convergence
0.2
0.4
0.6
0.8
1.0
1.2
1.4
1.6
1.8
2.0
damping
amplifying
network gain

figure 6

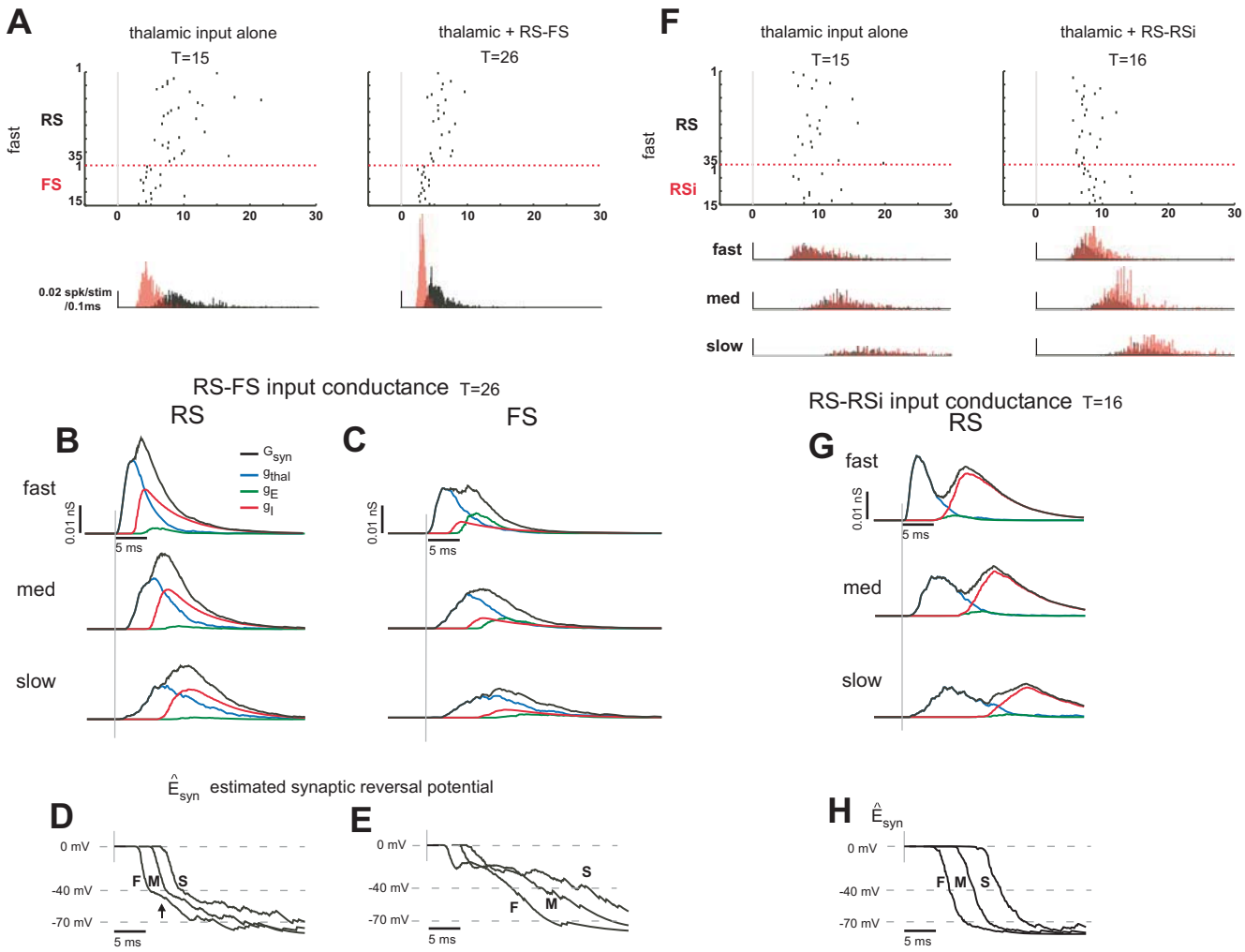
A
thalamic input alone
T=15
thalamic + RS-FS
T=26
fast
RS
FS
0.02 spk/stim
/0.1ms
F
thalamic input alone
T=15
thalamic + RS-RSi
T=16
RSi
fast
med
slow
RS-FS input conductance T=26
RS
FS
B
C
fast
med
slow
0.01 nS
5 ms
RS-RSi input conductance T=16
G
D
E
H
estimated synaptic reversal potential
0 mV
-40 mV
-70 mV
F
M
S

figure 7

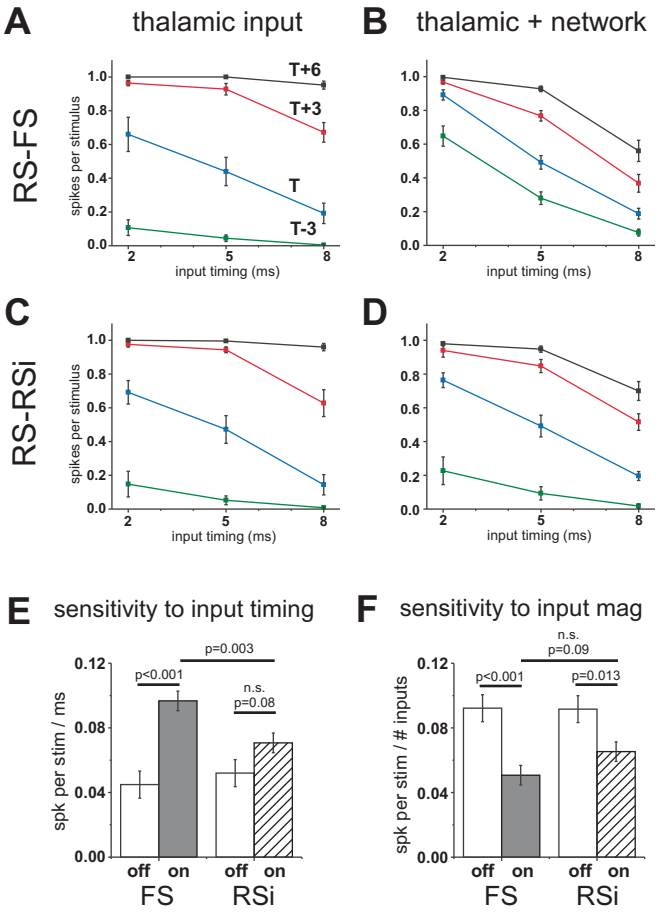
A
thalamic input
B
thalamic + network
RS-FS
RS-RSi
C
D
spikes per stimulus
input timing (ms)
T+6
T+3
T
T-3
E
sensitivity to input timing
F
sensitivity to input mag
spk per stim / ms
spk per stim / # inputs
p<0.001
p=0.003
n.s.
p=0.08
n.s.
p=0.09
p=0.013
off
on
FS
RSi

figure 8

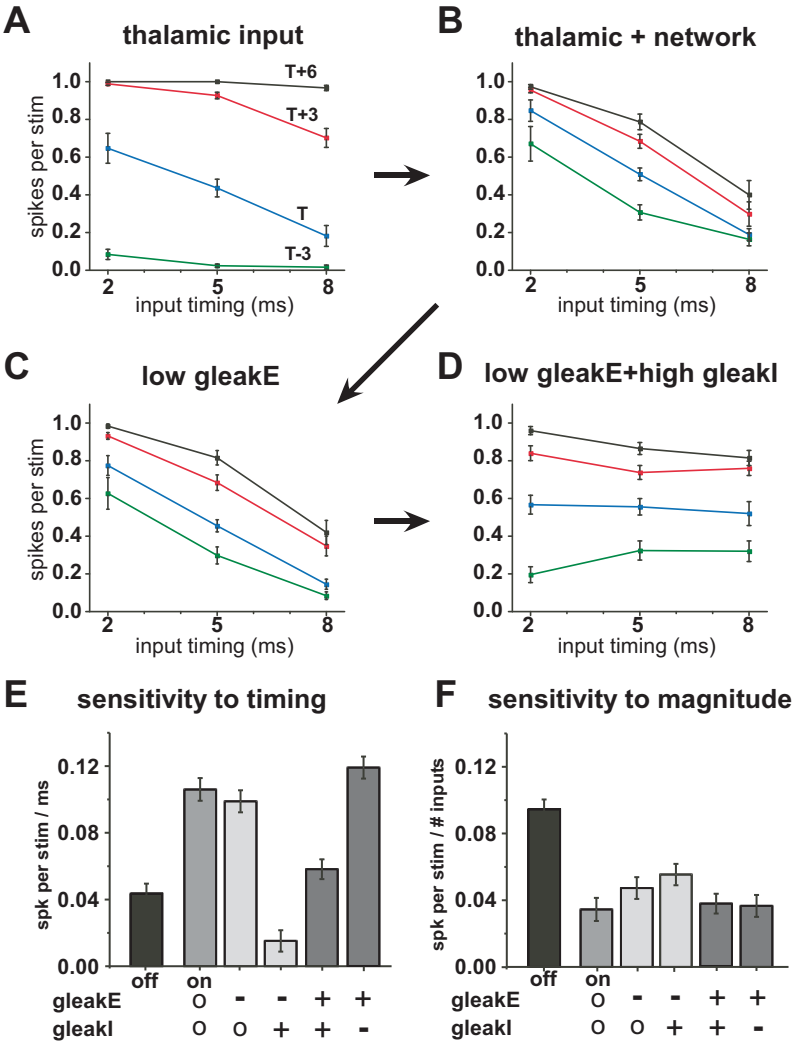
A
thalamic input
B
thalamic + network
C
low gleakE
D
low gleakE+high gleakI
E
sensitivity to timing
F
sensitivity to magnitude
spikes per stim
input timing (ms)
T+6
T+3
T
T-3
spk per stim / ms
spk per stim / # inputs
off
on
gleakE
gleakI

figure 9

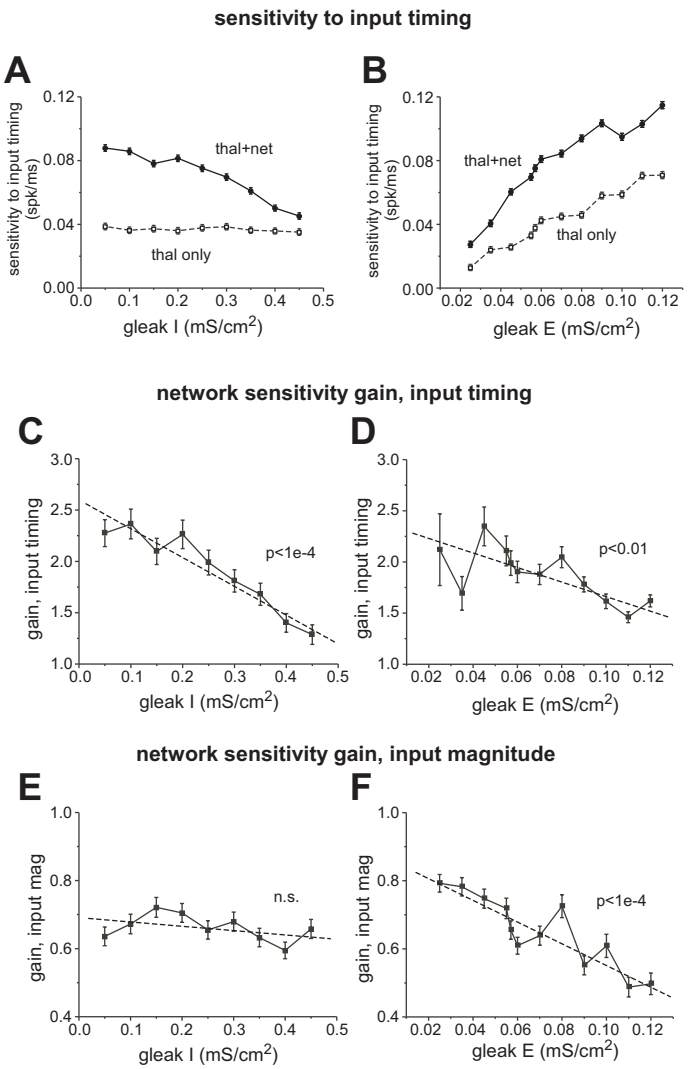
sensitivity to input timing
A
B
sensitivity to input timing (spk/ms)
thal+net
thal only
gleak I (mS/cm2)
gleak E (mS/cm2)
network sensitivity gain, input timing
C
D
gain, input timing
p<1e-4
p<0.01
network sensitivity gain, input magnitude
E
F
gain, input mag
n.s.
p<1e-4

figure 10

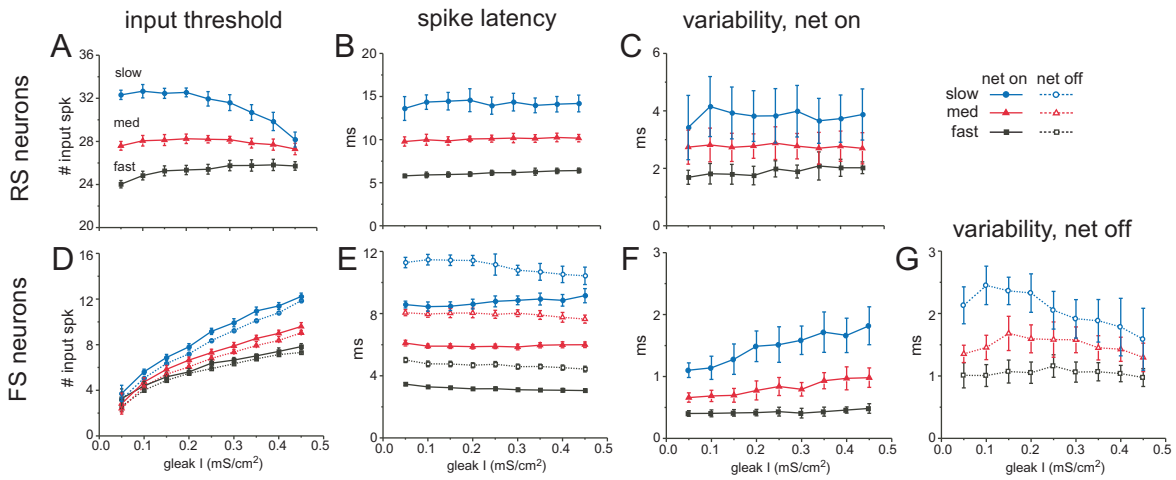
input threshold
spike latency
variability, net on
variability, net off
RS neurons
FS neurons
A
B
C
D
E
F
G
slow
med
fast
net on
net off
# input spk
ms
gleak I (mS/cm2)

figure 11

**Table 1**

| | | in vitro | | sim | |
|---|---|---|---|---|---|
| | | net OFF | net ON | net OFF | net ON |
| mean | threshold (# spikes) | 16.7 ± 0.8 | 29.0 ± 1.7 * | 14.6 ± 0.04 | 24.9 ± 0.06 * |
| | latency (ms) | 9.8 ± 0.4 | 6.8 ± 0.15 * | 13.3 ± 0.1 | 9.6 ± 0.04 * |
| | variability (ms) | 1.95 ± 0.17 | 1.11 ± 0.08 * | 3.21 ± 0.07 | 2.38 ± 0.05 * |
| sens. input timing | threshold (# spikes) | 0.41 ± 0.02 | 3.11 ± 0.33 * | 0.32 ± 0.02 | 0.86 ± 0.02 * |
| | latency (ms) | 1.27 ± 0.10 | 1.00 ± 0.03 * | 1.43 ± 0.03 | 1.23 ± 0.02 * |
| | variability (ms) | 0.28 ± 0.04 | 0.19 ± 0.02 * | 0.22 ± 0.02 | 0.24 ± 0.02 * |
| sens. input mag | latency (ms) | 0.56 ± 0.15 | 0.02 ± 0.012 * | 0.65 ± 0.03 | 0.09 ± 0.01 * |
| | variability (ms) | 0.24 ± 0.11 | 0.03 ± 0.011 * | 0.23 ± 0.03 | 0.03 ± 0.013 * |